Applied Catalysis A: General, 256 (2003) 1-2, 291-317

The Structure of Molybdenum-Heteropoly-Acids under Conditions of Gas Phase Selective Oxidation Catalysis: A Multi-Method in situ Study.

F.C. Jentoft, S. Klokishner, J. Kröhnert, J. Melsheimer, T. Ressler, O. Timpe, J. Wienold, R. Schlögl*

Department of Inorganic Chemistry, Fritz-Haber-Institute of the MPG, Faradayweg 4-6, 14195 Berlin, Germany

* Corresponding author: e-mail acsek@fhi-berlin.mpg.de, phone +49 30 8413 4400, fax +49 30 8413 4401

Recieved 11 February 2003; accepted 25 March 2003

Abstract

The present study focuses on the evidence about the existence of Keggin ions under various reactive conditions. The stability of the hydrated parent heteropoly acid (HPA) phases is probed in water, by thermal methods in the gas phase, by in situ X-ray diffraction and in situ EXAFS. An extensive analysis of the in situ optical spectra as UV-Vis-NIR in diffuse reflectance yields detailed information about the activated species that are clearly different from Keggin ions but are also clearly no fragments of binary oxides in crystalline or amorphous form. Infrared spectroscopy with CO as probe molecule is used to investigate active sites for their acidity. Besides –OH groups evidence for electron-rich Lewis acid sites was found in activated HPA. All information fit into a picture of a metastable defective polyoxometallate anion that is oligomerised to prevent crystallisation of binary oxides as the true nature of the "active HPA" catalyst. The as-synthesized HPA crystal is thus a pre catalyst and the precursor oxide mixture is the final deactivated state of the catalyst.

Keywords: diffuse reflectance, polyoxometallate, deactivated, in situ, thermal analysis, EXAFS, XRD, UV-vis-NIR spectroscopy, semi-empirical theory, FTIR spectroscopy, CO adsorption

Introduction

Vanado-molybdo-phosphates of the type of $H_4PVMo_{11}O_{40}*yH_2O$ (HPA) and $H_{4-x}Cs_x$-$PVMo_{11}O_{40}*yH_2O$ (Cs_xA, x=1-4) have been extensively studied as active catalysts for the selective oxidation of several alkanes, aldehydes and acids [1,2,3,4,5,6]. These compounds contain networks of MO_6 (M=V, Mo) octahedra, which resemble discrete fragments of metal oxide structures [7]. The Mo and V ions are distributed randomly in the mixed HPA and Cs_xA compounds. Structural studies revealed that the vanadium may be in the primary structure in the as-synthesized state, but is definitively located in the secondary structure as a vanadyl group after the HPA was used as catalyst [8,9].

HPA crystallize with a large number of water molecules that are present in two distinctly different forms: crystal and structural water. Water is lost under the action of a gas stream at 300 K and/or when temperature rises. The widths of the distribution of desorption temperatures and their starting points depend on sample composition (structure) and on experimental conditions (kinetics). After the removal of crystal and constitutional water further oxygen evolution takes place and the systems undergo internal redox reaction [10]. This complex reactivity that is partly reversible with temperature calls for an in-depth structural study in order to identify the true nature of the catalytically active material. Only then the often-quoted chemical diversity of HPA systems can fully be exploited for catalytic applications.

Central to redox catalysis is the knowledge of the electronic structure of the active phase. This can be studied in situ using optical spectroscopy. An essential advance in the studies of optical spectra of catalysts of different stages of their transformation was achieved by applying the in situ diffuse

reflectance UV/Vis/near-IR spectroscopy (DRS) [10,11], which proved to be a suitable technique for probing both d-d and charge transfer transitions at reaction temperature and under realistic gas compositions [12]. A number of groups have reported exsitu optical spectra [13,14,15,16,17]. It is known from these studies that the DRS method detects even small changes in spectral features connected with water loss or chemical reduction. This method was applied to investigate the reduction-reoxidation of HPA and Cs_2A by methanol and ethanol and to correlate structural changes with catalytic data [18].

The method exhibits limitations similar to those of other optical methods. The optical bands arising from intra- and interatomic transitions exhibit significant widths and thus limited resolution. Due to strong coupling of outer valence electronic states with the vibrational states of the solid the bands are additionally broadened. A further loss in resolution caused by data acquisition above room temperature has to be accepted as consequence of the dynamic nature of the activated systems [11,19]. The multiple redox states of activated HPA give rise to band systems strongly overlapping and thus requiring data analysis based on theoretical predictions in order to derive meaningful electronic structural information.

The parent structures of HPA that constitute highly active materials for selective oxidation reactions (e.g. methacrolein to methacrylic acid [20]) contain as common motif the Keggin anion. Incompletely salified Cs_xA (e.g. $Cs_xH_{3-x}[PMo_{12}O_{40}]$ ($2 \leq x < 3$), *Pn*-3*m* (No. 244), a = 11.85 Å [21]), for instance, is applied on the industrial scale. It has been proposed that the active phase of the HPA under reaction conditions corresponds to the intact and undistorted Keggin structure and, hence, that the catalytic reactivity of the material could be understood based on the initial structure of the HPA [22,23]. Conversely, the stability of the Keggin anions during thermal treatment and under catalytic conditions, the homogeneity of the partially salified HPA, and the correlation of the structure of the HPA and its catalytic activity are under debate [24,25,26,27]. Mixed phases of partially salified HPA have been proposed forming a core-shell system of the Cs_3A-salt and the free acid under catalytic conditions [25]. Furthermore, it has been suggested that the molybdenum cations [28] as well as the vanadium cations [29,30] migrate from the Keggin anion to cationic positions in the structure [31,32] and that the heteropoly acids become partially reduced under reaction conditions [33,34].

This migration of cations from the Keggin anion has been speculated to be responsible for the catalytic activity of the heteropoly oxomolybdates with Keggin structure [25,29,30,33,35,36,37]. The result of the migration is a cubic molybdenum autosalified heteropolyacid (*Pn*-3*m*, a = 11.853 Å) derived from triclinic $H_3[PMo_{12}O_{40}]*13H_2O$ under reduction conditions with propene and hydrogen at temperatures above 600 K. This way the in situ studies on the electronic structure of the active state of HPA are corroborated by direct in situ geometric structural studies using X-ray diffraction and EXAFS.

Redox transformations require in addition to the availability of electrons (that are absent in stoichiometric parent HPA) certain acid-basic properties of the bi-functional catalysts. A frequently cited property of HPA is their strong acidity that is related to the presence of structural water. As this water may be absent under reaction conditions it is adequate to probe the acid-base properties of activated samples with a suitable method. The acidity of solid heteropoly compounds [38] has been investigated through interaction with bases combined with different methods of analysis: (i) Hammett indicators + visual inspection [39], (ii) ammonia + temperature programmed desorption (TPD) [40,41], IR spectroscopy [42], calorimetry [43,44], and (iii) pyridine + TPD, IR spectroscopy [45,46].

The use of Hammett indicators is difficult because many heteropoly compounds are strongly colored. Not only the surface of heteropoly acids interacts with vapors; many polar molecules enter the bulk, usually in a number related to the amount of protons per formula unit [47] (formation of clathrates?). The reaction with the strongly basic molecules ammonia and pyridine leads to the stoichiometric formation of ammonium and pyridinium salts. This reaction is not easily reversible by evacuation at moderate temperatures. Ammonium salts only start to decompose at higher temperature, e.g. $(NH_4)_3PMo_{12}O_{40}$ releases most of its NH_3 at 700 K [41]. Upon heating pyridinium salts of $H_{3+x}PMo_{12-x}V_xO_{40}$ in TPD experiments H_2O, CO, CO_2, and N_2 were detected besides pyridine, indicating that a fraction of the pyridine was oxidized. The strong bases ammonia and pyridine can, thus, not be considered as probe molecules for the heteropoly compounds within the definition of acidity as constituting an equilibrium reaction between a conjugated acid-base pair. The heat measured during interaction with the "probe" is actually the heat for the salt formation. It is thus possible to estimate the difference in the enthalpies of formation between the acid and the salt. The often discussed difference in stability can be quantified; as an example $(NH_4)_3PMo_{12}O_{40}$ is about 270 kJ mol^{-1} more stable than the corresponding acid.

The salt formation interferes with the detection of further acid sites, because all additionally offered probe molecules interact with the ammonium or pyridinium salt and not with the original compound. Ammonia and pyridine are thus good to titrate the acidic protons, but all further interpretations are questionable. Bielański et al. [43] only found Brønsted and no Lewis sites on a series of $H_{3+x}PMo_{12-x}V_xO_{40}$ samples using ammonia as a probe, equally Serwicka et al. [47] detected ad(b)sorbed pyridine “predominantly” in its protonated form after adsorption on $H_{3+x}PMo_{12-x}V_xO_{40}$.

Another probe tested was carbon monoxide, which was adsorbed at 100 K on $H_3PMo_{12}O_{40}$ and its cesium salts [48]. The spectra showed three different bands at 2165 cm^{-1}, assigned to adsorption on OH groups, 2154 cm^{-1}, assigned to adsorption on cesium cations, and 2139 cm^{-1}, assigned to physisorbed species. Again, no Lewis sites were found. However, as HPA are thought to activate oxygen through a Mars–van–Krevelen mechanism [10,42], the presence of

oxygen vacancies and, thus, Lewis acid sites, i.e. coordinatively unsaturated (cus) cations, appears plausible.

Experimental

Synthesis

$H_{3(4)}P(V)Mo_{12(11)}O_{40}$ was prepared by dispersing MoO_3 (and V_2O_5, both obtained from Merck) in distilled water. Addition of an excess amount of phosphoric acid and refluxing led via dissolution-precipitation to the HPA. Silicon containing HPA were synthesised by dissolving sodium molybdate (and sodium vanadate, both Merck) in distilled water and adding sodium silicate. An alkaline solution was obtained, which was then slowly acidified with hydrochloric acid. From these solutions, the free HPA were extracted with diethyl ether. The heteropoly compounds, $H_3[PMo_{12}O_{40}]*13H_2O$ and $Cs_2H[PMo_{12}O_{40}]$, were prepared following the method described by Tsigdinos et al. [49]. All Cs salts of the HPA were obtained by addition of Cs_2CO_3 to a solution of the appropriate HPA in distilled water. The solution was stirred and subsequently reduced until complete precipitation. The main component that was obtained was $Cs_3HPMo_{12}O_{40}$. A molybdenum salified HPA was obtained by thermal treatment of $H_3[PMo_{12}O_{40}]*13H_2O$ in a flow reactor in the gas phase of 10% propene in helium (100ml/min total flow) up to 673 K (5 K/min). A series of salts with the general composition $(NR_4)_2H_2[PVMo_{11}O_{40}]*nH_2O$ was obtained by precipitating the free acid form with alkylammonium bromides. The alkyl group (R) was -H, -methyl, -ethyl, -*n*-propyl or -*n*-butyl. All samples were checked for phase purity by X-ray diffraction. A careful study of the intensity distribution and search for amorphous constituents were applied. Only well-crystalline materials were used in the subsequent studies. This way reproducibility of the samples as further checked by thermal analysis was sufficient over the last 10 years that were needed to arrive at the results presented here.

Analytical

Stability in water

Conductivity was measured with a cell exhibiting a cell constant of 1 cm^{-1} and a WTW device; the Zr(IV) solution was added manually in small quantities and the corresponding conductivity values were noted; the solution was kept at room temperature during the titration;

TG

The TG-investigations were carried out using a Seiko SSC 5200; about 20 mg of sample were placed in an Al-pan; the set-up allowed the control of atmosphere and a constant gas-stream of desired composition passing over the heated sample (realized by the use of BRONKHORST mass-flow controllers); the detection of gaseous species was carried out with an IMR-MS (ion-molecule-reaction excitation mass spectroscopy [50]) device connected to the exhaust of the TG-instrument; the heating rate was set to 5 or 10 K/min.

TPRS

Experiments were conducted in a tubular glass reactor, inner diameter approximately 7.9 mm; about 20 mg of sample were fixed by glass wool; a stream of He was added to the reactant gases to give a total flow of 100 ml/min; analysis of gaseous compounds downstream of the reactor wss realized by a conventional *QMS Prisma* (BALZERS/PFEIFFER) connected to the exhaust.

In-situ TG-DSC

Investigations were performed using a NETZSCH device; the sample was placed in vertical tubular reactor and a gas stream was forced to pass around the sample; the gas flows were regulated by BRONKHORST mass-flow controllers.

In situ X-ray diffraction

In situ XRD experiments were performed on a STOE STADI P powder diffractometer (Bragg-Brentano geometry, secondary monochromator, Cu-Kα radiation) equipped with a Bühler HDK S1 high temperature chamber.

In situ XAS

In situ transmission XAS experiments were performed at the Mo K edge (19.999 keV) at beamline X1 at the *Hamburg Synchrotron Radiation Laboratory*, HASYLAB, using a Si(311) double crystal monochromator (measuring time ~ 4.5 min/scan): The measurements were performed in a flow reactor (4 ml volume) in the transmission geometry. Total flow of gases was set to 20 ml/min (10% propene in helium) and a heating rate of 5 K/min was applied. Analysis of the gas phase was performed with a quadrupol mass spectrometer, *QMS 200* (*Pfeiffer*), with a time resolution of ~12 s per selected masses scan. The heteropoly acid was mixed with boron nitride (7 mg HPA, 30 mg BN) and pressed with a force of 1 ton into a 5 mm diameter pellet resulting in an edge jump at the Mo K-edge of $\Delta\mu_x \sim 2$. Details of the experimental set up can be found in Ref. [50]. XAFS data reduction and analysis were performed using the software WinXAS 2.3. [51].

EXAFS data analysis was performed using theoretical backscattering phases and amplitudes calculated with the ab initio multiple scattering code FEFF7 [52]. EXAFS refinements were performed in R space to magnitude and imaginary part of a Fourier transformed k^3-weighted experimental $\chi(k)$ using the standard EXAFS formula (k range from 4.3 to 14.9 $Å^{-1}$, R range 0.7 to 4.2 Å). Structural parameters that are determined by a least-squares EXAFS fit to the experimental spectra are (i) one E0 shift, (ii) Debye-Waller factors for single-scattering paths, (iii) distances of single-scattering paths. Coordination numbers (CN) and S_0^2 were kept invariant in the refinement.

In-situ UV-Vis-near-IR spectroscopy

A description of the modified UV-Vis-near-IR diffuse reflectance spectrometer, the home-made flow-through microreactor and other experimental details can be found elsewhere [10,12]. All spectroscopic measurements were

carried out with Spectralon® (Labsphere) as reference material. HPA samples (7-19 wt%) were mixed with SiO_2 (Heraeus, 0.1-0.4 mm). The apparent absorption $K(\lambda)$ as a function of the wavelength λ was evaluated from the diffuse reflectance data using the Kubelka-Munk rule, which was shown to yield superior results than the intensity scaling with 1- $R_{mixture} / R_{SiO_2}$.

IR spectroscopy and CO adsorption

The IR experiments were carried out on a Perkin Elmer S 2000 spectrometer equipped with a liquid nitrogen cooled MCT detector at a spectral resolution of 4 cm^{-1} and accumulation of 200 scans. The samples were pressed (at 320 MPa) into infrared transparent, self-supporting wafers (typically 20 to 30 mg/cm^2) which were placed in a home-made stainless steel, low-temperature infrared cell with CaF_2 windows. The cell was connected to a vacuum system. The sample was activated in situ in the heating zone of the IR cell under vacuum (final pressure $1x10^{-4}$ hPa) at 523 and 673 K for 2.5 h (subsequent experiments with one sample). The spectra were recorded at 77 K while the CO pressure was increased stepwise in the range of 0.001 – 6.5 hPa. All spectra shown represent the difference between spectra of the sample recorded in the presence and in the absence of CO.

Results and Discussion

Stability

Stability in water

Keggin-type HPA are stable in aqueous solution only at a pH lower than 3. A rise in pH decomposes the complex anion and smaller metallate units are formed. It is argued, that even at low pH the HPA compounds are subjected to dynamic equilibria rather than to permanently stable molecular entities. This can be demonstrated by elimination of PO_4^{3-} from a solution of [PMo] by precipitation with $ZrOCl_2$ which is known to produce insoluble solids of the approximate composition $Zr_3(PO_4)_4$ even in very acidic environments. A cloudy precipitate formed instantaneously upon the addition of the first quantities of a 0.01 M $ZrO(SO_4)$ solution to the 0.01 M dissolved [PMo]. After drying at room temperature the isolated solid was a mixture of an amorphous phase and of $Zr_3(PO_4)_4$ in the XRD characterisation.

The action of the precipitating agent on the solution was investigated by the course of the ionic conductivity of the solution during Zr addition. Results are presented in Figure 1. Regardless of the immediate precipitation and the formation of $Zr_3(PO_4)_4$ the evolution of the conductivity (κ) does not show the characteristic features of the comparative H_3PO_4 titration (inflection point at the stoichiometric ratio Zr:P = 0.75) but a monotonous increase over the whole range. The HPA is a very strong acid with pKa values below 1 and fully dissociated. The rise in conductivity in parallel to the formation of an insoluble fraction therefore indicates the generation of smaller entities by the degradation of the complex Keggin anion. This simple experiment shows clearly the structural dynamics of Mo-HPA even in water at 300 K.

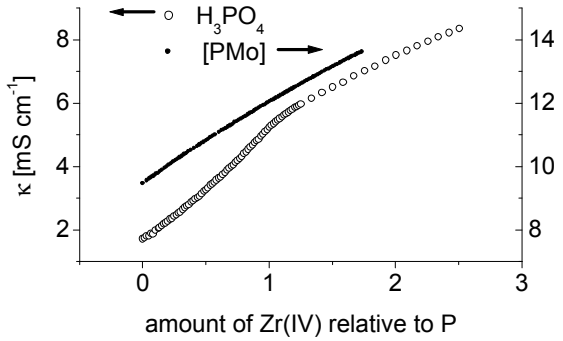

Fig. 1 The specific conductivity (κ) of a $H_3[PMo_{12}O_{40}]$ solution (solid symbols) and H_3PO_4 (open symbols) as response of the addition of $ZrO(SO_4)$; the initial concentration of $H_3[PMo_{12}O_{40}]$ 7.15 mM and of H_3PO_4 7.38 mM; the amount of added Zr (IV) is noted in terms of the Zr:P ratio.

Thermal stability of P and Si- HPA

The decomposition and reduction of HPA under partial oxidation reaction conditions is demonstrated by thermogravimetry. Figure 2 summarises characteristic results. The first

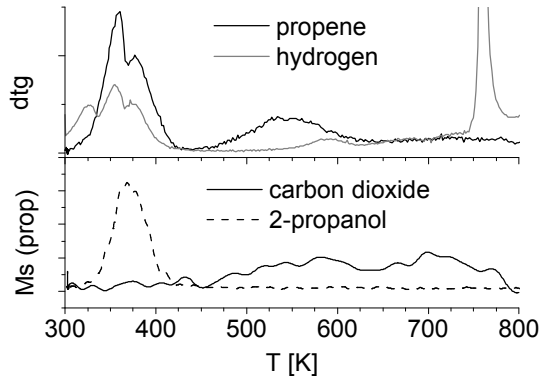

Fig. 2 TG-MS investigation on $H_4[PVMo_{11}O_{40}]$ in reducing atmospheres: 50 % hydrogen (gray) and 25 % propene (black), heating rate 5 K/min; the DTG-curves are displayed above and the MS traces of carbon dioxide (m/e=44) and 2-propanol (m/e=45) corresponding to the run in propene atmosphere below.

two peaks in the DTG can be attributed to loss of crystal water (up to 400K) and subsequent irreversible expulsion of the structural water (up to 640K), which initializes the reduction of the acid itself. Dehydration in hydrogen atmosphere leads, as shown in Figure 3, to three different steps in the TG curve corresponding to three different hydrates. Propene, a model educt for selective oxidation to acrolein and acrylic acid, reacts already at room temperature with the crystal water of the acidic HPA leading to 2-propanol. This way the loss of water of the HPA samples is considerably

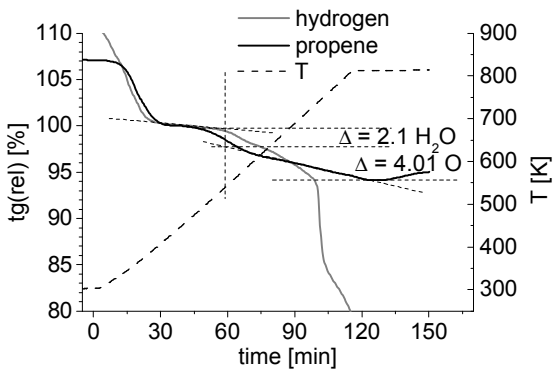

Fig. 3 TG investigation on $H_{3(4)}P(Si)Mo_{12}O_{40}$ and $H_{4(5)}Si(P)VMo_{11}O_{40}$ in 50% hydrogen (gray line) and 25 % propene (black line); heating rate 5 K/min; the temperature (dashed line) is noted on the right axis; the mass of the dehydrated acid is set to 100 %.

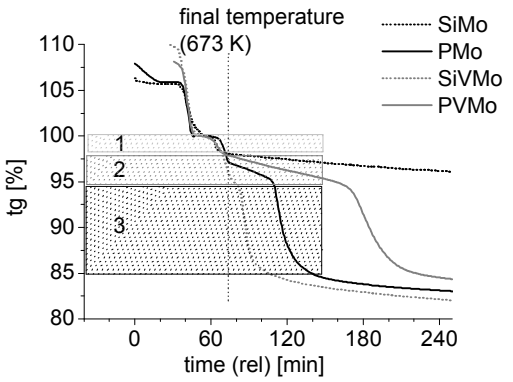

Fig. 4 TG investigation on $H_4[(P/Si)VMo_{11}O_{40}]$ in 50 % hydrogen atmosphere; heteroatom P (solid lines) and Si (dotted lines), one addenda molybdenum atom substituted by vanadium (gray lines) and no vanadium (black lines); the temperature is initially increased with 10 K/min to reach the final value at 75 min on the relative scale. The indicated ranges of reaction correspond to the following weight losses: (1)=structural water, 2%; (2)=initial reduction, 3.4%; (3)=further reduction of decomposition products, 10%.

increased and occurs already at room temperature. HPA are not reduced at all at 300 K by hydrogen.

Figure 3 reveals quantitatively the effects of the loss of structural water and of further thermal reduction. In propene the loss of structural water is shifted to lower temperatures as compared to the analysis in hydrogen. The resulting defects are presumably the reason for the low reaction barriers of subsequent structural reorganization of the Keggin anions. The next reduction step (up to 730K) involves the loss of four oxygen atoms per Keggin unit that react with propene. Whilst hydrogen reduction leads to complete removal of all oxygen from the metals, there is no further reduction by propene. The isothermal episode at 800 K shows that this difference is not due to kinetic hindrance. The gain in mass of the sample in propene is due to carbon deposition as evidenced by subsequent TPO (data not shown).

Influence of the heteroatom P or Si on thermal stability

A similar experiment was carried out with HPA with different heteroatoms. In Figure 4 the results are shown of a linear heating experiment in hydrogen up to 673 K followed by an isothermal episode at that temperature to simulate thermal load under catalytic conditions. The losses of crystal and structural water occur as observed in Figure 3 and show no specific effect related to the inner heteroatom of the Keggin units. The reduction of the HPA starts immediately after complete elimination of crystal and structural water, as these systems do not possess a stability plateau after water removal. The process can be divided into two steps. The first step is kinetically controlled and corresponds to removal of four oxygen atoms. It may be assumed that these four atoms are directly co-ordinated to the heteroatom P or Si as can be seen from the significant effect of its alteration. A continuous mass loss of the P-containing samples is observed after the loss of structural water under isothermal conditions in hydrogen atmosphere. It is attributed to the loss of P in form of reduced P-compounds, e.g. PH_3.

Directly after this mass loss, the TG curves show a step, which is attributed to the reduction of the transition metal ions. The HPA containing phosphorous are more stable than the ones containing silicon. The incorporation of V into the Keggin cage leads to enhanced destabilization in the case of Si-HPA. Investigations of the catalytic activity (TPRS) can be correlated with the TG data. All investigated HPA are active for the partial oxidation reactions only after they have lost all their structural water. This catalytic activity decreases with time on stream. The active fragments that were formed from the Keggin anions after loss of structural water are not stable under "dry" catalytic conditions, i.e. with no excess water in the feed. Total oxidation increases with the reactor temperature. For Si-HPA, the total oxidation is the major reaction path already after the loss of structural water. From a comparison of the catalytic activities and selectivities of the different materials it can be concluded that P stabilizes the fragments of the decomposed Keggin anions, being predominantly active in selective oxidation. The Si-containing catalysts seem to decompose into fragments more similar in structure to MoO_3 as concluded from the pronounced selectivity to total oxidation.

Stability of Cs- and ammonium salts in various atmospheres

The influence of the replacement of the acidic protons by cesium is demonstrated in Figure 5. It is important to investigate the isothermal behaviour at typical reaction temperatures following the linear heating to see kinetically hindered processes relevant for the longer-term stability of the materials. HPA preparations in which all protons of the HPA were exchanged by Cs^+ ions exhibited a considerably enhanced stability toward reduction. The complete salification suppresses the reduction of the metal oxides as it keeps to-

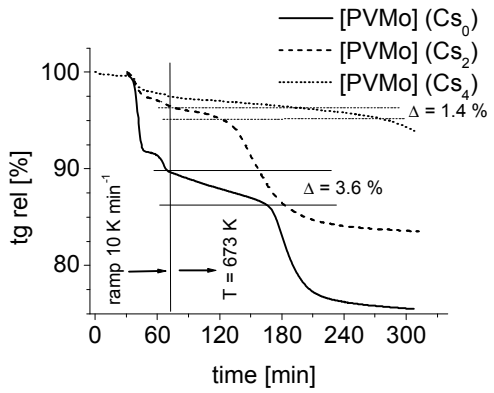

Fig. 5a TG investigation of $Cs_x[PVMo_{11}O_{40}]$; reduction in 50 % hydrogen; different degrees of neutralization: no acid proton replaced (solid line), 2 protons replaced by Cs^+ (dashed line) and all protons replaced (dotted line); the temperature is increased by 10 K/min to reach the final value of 673 K at 75 min on the relative scale; the relative mass loss for the Cs(x=0) and the Cs(x=2) samples after the expulsion of structural water is noted in the figure.

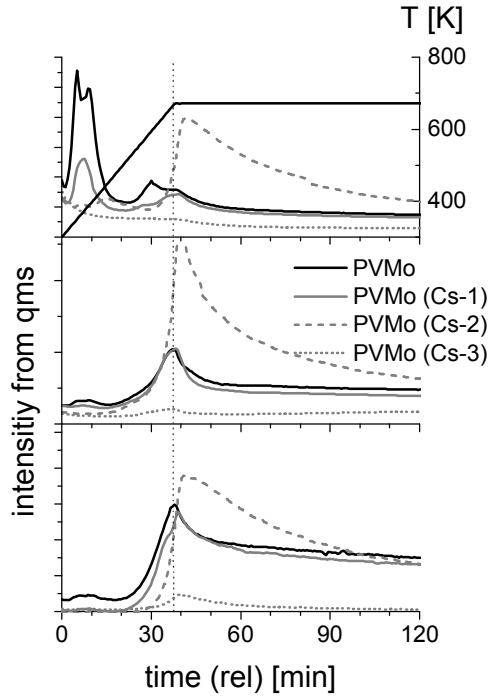

Fig 5b Temperature-programmed reaction spectroscopy (TPRS) investigation on Cs salts of $[PVMo_{11}O_{40}]$; feed composition: equimolar ratio of propene and oxygen, 10 % in He; the temperature is initially increased to 673 K by 10 K/min and held at this level over the further course of experiment as displayed on the right axis of the panel at the top; traces of gaseous products are detected by an IMR-MS device; top panel water (m/e=18), central panel carbon dioxide (m/e=44) and bottom panel acrolein (m/e=56); the free acid Cs (x=0) is indicated by black lines, the Cs salts by gray lines – Cs(x=1) (solid), Cs(x=2) (dashed), Cs(x=3) (dotted).

gether the Keggin oligomers at 673 K. The TG curve of Figure 5a shows that the HPA is stabilised by the introduction of Cs. These salts cannot liberate structural water. The decomposition and condensation of the Keggin anion fragments therefore are suppressed. Hence, these Cs salts are catalytically inactive for the partial oxidation. Whilst $Cs_3HPVMo_{11}O_{40}$ is the most stable of the samples it is also the least active (Fig. 5b). The highest activity is shown by the sample where Cs replaced two protons. Such systems exhibit vacancies in both cationic and anionic sublattices. Salts of this nominal composition precipitate first regardless the ratio of HPA to Cs^+ in the solution. Mixed solids form with a variable amount of Cs^+ per Keggin unit. This arrangement is thermally unstable and tends to segregate into a core shell-structure [24,25]. The formal composition of the Cs(2)HPA transforms during initial thermal treatment (drying above 473 K) into a nucleus, formed by the stable Cs(3)-salt and a shell of less stable but catalytically active phases of Cs(3-x) salts [24]. This arrangement can be considered as HPA supported on the Cs(3)-salt. The support enlarges the surface area and may stabilize active and metastable phases generated by a partial decomposition of HPA during activation procedures or under reaction conditions. This model is likely to explain the course of the catalytic activity in oxidation reactions along a series of Cs-HPA salts with different numbers of protons replaced by alkali ions.

Salts formed with bulky and instable cations

Replacing Cs^+ by ammonium ions offers additional opportunities for systematic variation. The availability of alkyl-ammonium species enables the systematic alteration of the cation size and in turn the stability of the HPA-salts. The oxidative sensitivity of organic ligands allows for strong auto-reduction upon thermal treatment and thus for changing the redox state of the HPA without addition of gas phase reagents. Due to the strong propensity of HPA to become reduced and hence defective in their internal structure the entire activation and deactivation scenario in temperature programmed reaction spectroscopy (TPRS) is shortened considerably as compared to Cs salts. The decomposing alkyl-ammonium salt will emit specific fragments depending on the nature of the attached organic residues. These fragments can be detected by mass spectroscopy and used as indicators for the decomposition of the Keggin structure.

A series of salts with the general composition $(NR_4)_2H_2[PVMo_{11}O_{40}]*nH_2O$ is subjected to temperature programmed reaction analysis (R: -H, -methyl, -ethyl, -n-propyl, -n-butyl). Characterization by TG (in inert atmosphere or in 50 % oxygen, heating rate 5 K/min) reveals a distinct dependence of the thermal stability upon the nature of the cation, i. e. upon the residue R. The DTG traces presented in Figure 6 reveal the sample with the bulkiest cation to be the least stable among the alkylammonium salts. The weight-loss is divided into three major events. At the lowest temperature the loss of crystal water occurs, manifested by the very weak DTG-signal around 370 K. The last and most intense DTG signal for all samples is attributed to complete decomposition, as confirmed by simultaneous analysis of the

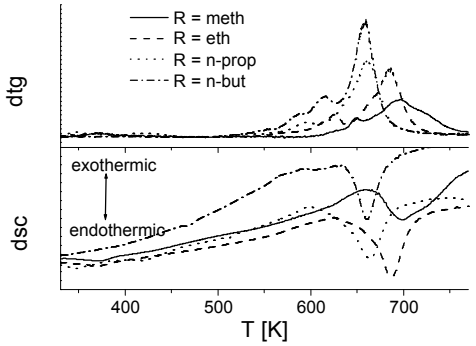

Fig 6 Alkylammonium salts of the composition $(NR_4)_2H_2[PVMo_{11}O_{40}]$ are subjected to thermal decomposition in He; heating rate: 5 K/min; the organic residue in the ammonium cation are varied. The DTG curves are displayed in the top panel, the corresponding DSC curves are given at the bottom panel.

volatile compounds by MS. This decomposition is an endothermic process in inert atmosphere as indicated by the DSC curves. A minor mass loss appears as intermediate event for all samples prior to the main decomposition peak. The underlying process reveals no pronounced energetic characteristic under the given conditions. The corresponding temperature ranges from 550 K for the least stable (R = n-butyl) sample to 650 K for the most stable (R = methyl) one. The analogy with the decomposition scheme shown by the Cs-salts of this HPA allows the identification of this step as the expulsion of structural water. The integrated weight losses corresponding to these DTG signals amount to 1 % and are in reasonable agreement with the assumed abstraction of structural water (note: the molecular mass of the HPA-compounds of concern ranges around 1800 g/mol and one molecule of water released will account for a mass loss of approximately 0,1 %). The loss of structural water is the beginning of the decomposition of the molecular anions. The threshold temperature for the disintegration is strongly affected by the whole salt structure and is not a function of the anion chemistry. This may be understood as kinetic hindrance of the evolution of water by the strength of the cation-anion interaction preventing microstructural disruption of the solid during water evolution.

The decomposition of the alkylammonium salts in reactant feed allows to link the occurrence of product gases and hence the catalytic activity to the degradation of the HPA crystals. The results of TPRS runs with an equimolar ratio of propene to oxygen in the feed are shown in Figure 7a–c for several relevant molecular constituents and in Figure 7d as the conversion of oxygen and propene, respectively. The applied heating ramp was set to 5 K/min. The detection of gaseous compounds downstream the reactor was performed using the highly structure-specific IMR-MS detector allowing the analysis of the products without the usual strong fragmentation [53]. The mass signals for water (18), carbon dioxide (44) and partially oxidized products (59) are displayed. As a general feature the onset temperature for the

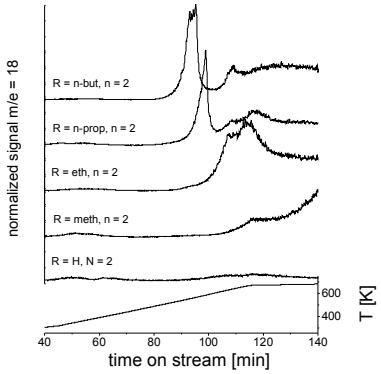

Fig. 7a TPRS (water m/e=18) of alkylammonium salts of the composition $(NR_4)_2H_2[PVMo_{11}O_{40}]$; feed composition: equimolar ratio of propene and oxygen; detection of products by IMR-MS; heating rate: 5 K/min.

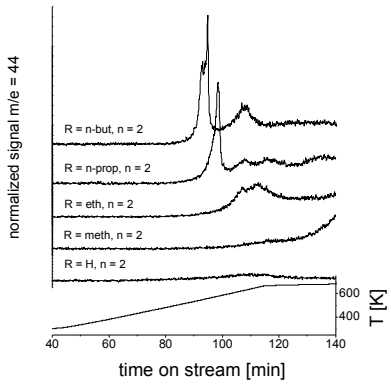

Fig. 7b TPRS of samples from Fig. 7a (carbon dioxide m/e=44).

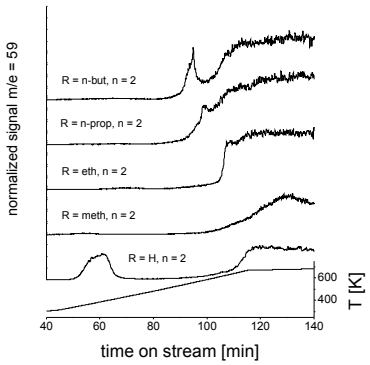

Fig. 7c TPRS of samples from Fig- 7a (products of partial oxidation m/e=59).

appearance of these compounds is shifted upwards as the size of the ammonium cation is decreased. The samples are developing their catalytic activity only upon their destruction. The comparison of the calculated conversion in oxygen and propene reveals, that the first, very sharp maximum in carbon dioxide and water for the samples with (-butyl) and

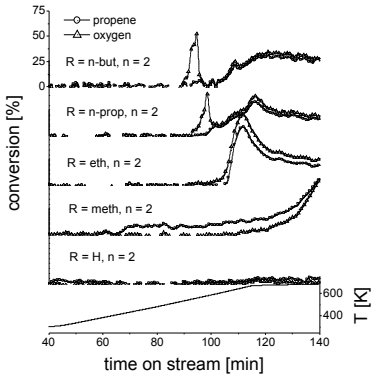

Fig. 7d TPRS of samples from Fig. 7a (conversion of educts oxygen (triangles) and propene(circles)).

(-propyl) at about 600 K is caused exclusively by the oxidation of the sample consuming oxygen and not by the reaction of gas-phase propene. Furthermore these data confirm the generation of selectively active species from the decomposition of the initial HPA structures. The term selectivity is understood as the ratio of partial oxidation products to the products of total combustion. The behaviour of the relatively stable (-methyl) sample is remarkable as even at 673 K the decomposition proceeds rather slowly. This is accompanied by a continuous rise in conversion. On the other hand, the amount of partial oxidation products passes through a maximum during completion of the HPA disintegration. This observation points to the metastable and transient character of the phases responsible for partial oxidation.

The additional information to TPRS gained by thermogravimetric analysis in inert and oxidizing atmospheres can elucidate the processes further. This is demonstrated for the

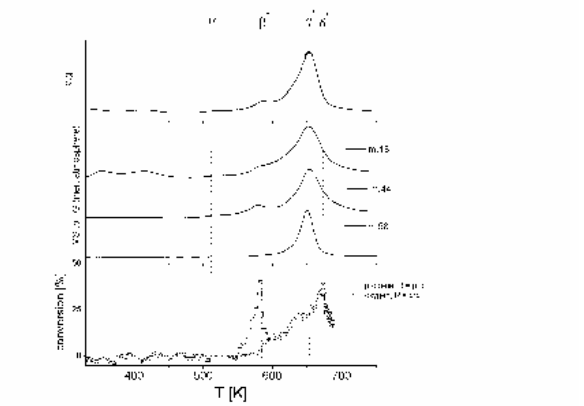

Fig. 8 Comparison of TG/MS (inert atmosphere) to TPRS (propene : oxygen = 1 : 1). Results for the alkylammonium salt $(NR_4)_2H_2[PVMo_{11}O_{40}]$ with R = n-propyl; heating rate is 5 K/min for all. The DTG-curve is at the top, the detected MS-signals corresponding to the TG-run are in the middle, and at the bottom the estimated conversions for the same sample in the TPRS-experiment are given; important sections are indicated by vertical lines and referred to in the text.

(-propyl) sample in Figures 8 and 9. The points α, β γand δ indicate significant events and will be discussed briefly. In between the markers α and βthe sample loses the structural water, best seen for the oxidizing atmosphere in Figure 9.

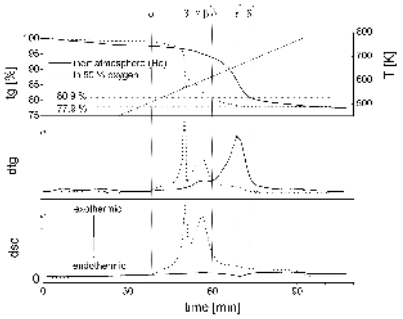

Fig. 9 Comparison of TG/DSC investigations on the sample $(Nprp_4)_2H_2[PVMo_{11}O_{40}]$ in inert atmosphere (He) and in oxidizing atmosphere (dotted lines) (50 % oxygen in He); heating rate is 5 K/min; in the top-panel: course of the relative mass and of the temperature (right axis); central panel: DTG signals; bottom panel: DSC signals. Important sections are indicated by vertical lines and referred to in the text. Lines γ and β^* coincide.

The expulsion of structural water is followed by the decomposition of the (N-propyl) cations. In the presence of atmospheric oxygen, this decomposition is strongly exothermic (note the corresponding DSC peaks and the deviation in the temperature ramp). This is not a single step and gives rise to at least two signals (β and γ). In inert atmosphere, these steps are shifted to higher temperatures and occur as endothermic (β^* and γ^*) reactions, since no external combustion of ligands can occur. Coinciding with step β^* (inert atmosphere), water and carbon dioxide were detected (by QMS) in the He stream. Clearly, already during this initial step, the organic residue is partly subjected to internal combustion by autoreduction of the HPA detectable by a corresponding weight loss. If oxygen is available in considerable concentrations (10 %), pronounced oxidation of the organic residue is observed at this initial stage. So far, the sample did not collapse completely. This is what happens at the γevent, the sample restructures and presumably changes its internal Keggin structure as the counterions disappear. The signal of m/e=58 detected in the inert atmosphere is typically a $N\text{-}C_3$ fragment, released upon the total disintegration of the alkylammonium ion. The simultaneous appearance of carbon dioxide and water in the inert atmosphere proves the reduction of the oxides. This assignment agrees with the identification of MoO_2 by XRD in the material after the TPRS experiment.

The conversion of propene in the TPRS run is the highest at point δ. This is seen as the consequence of the initial HPA precatalyst restructuring. The residual mass of the sample decomposed in 50 % oxygen (77.9 %) is in very good agreement with the mass calculated for the formation of MoO_3 and V_2O_5 as final compounds. As observed for other

Keggin-type HPA, a slow process takes place before the reorganization to the final decomposition products occurs. The weight loss of 3 % (from 80.9 % to 77.9 %) corresponds exactly to the abstraction of 4 oxygen atoms per formula unit and most probably indicates the detachment of the triads from the central heteroatom. The triads of octahedra restructure into intermediate states first forming lacunary structures and upon the loss of the "templating" central tetrahedron into binary oxides if sufficient oxygen excess is present. The comparison with the conversion data displayed in the lower part of Figure 8 allows to ascribe the maximum catalytic activity to the partially decomposed (probably lacunary) Keggin ion and the following deactivation to the detachment from the central tetrahedron facilitating the formation of poorly active ordered binary oxides.

In situ structural studies

The previous chapter revealed strong evidence for the view that at least in gas-phase oxidation catalysis the HPA systems are not active in their parent state known from X-ray diffraction studies. The massive dependence of the sequence of events and the complexity of the thermal degradation behaviour that is critically related to catalytic performance require the re-determination of HPA structures under reaction conditions. The powder X-ray diffraction analysis of used catalysts showed binary oxides in their highest or an intermediate oxidation state depending on the chemical potential of the reaction atmosphere. Evidence was presented that the good catalytic performance of these systems is indeed related to a metastable intermediate assigned from weight changes to "lacunary" structures, i.e. to voids in the spherical Keggin motif. For this reason a combination of methods is chosen sensitive either to long-range order and the packing of potentially defective Keggin units or to the local chemical environment of the M-O polyhedra that is sensitive to the partial destruction of the anions.

In situ X-ray diffraction

The evolution of the long-range structure of $H_3[PMo_{12}O_{40}]*13H_2O$ during thermal treatment in 10 % propene in helium was measured by in situ X-ray diffraction (XRD). Selected XRD patterns measured at 315 K, 373 K, and 723 K are depicted in Figure 10. At 315 K the 8-hydrate [27,28] is detected together with the anhydrous $H_3[PMo_{12}O_{40}]$ [54]. The 8-hydrate is formed from the initial 13-hydrate in the temperature range of 300 - 315 K. Between 348 and 573 K the anhydrous phase is observed, while at 598 K a highly disordered and not yet identified phase is formed. The latter is slowly transformed into the cubic HPA (*Pn*-3*m*, *a* = 11.853 Å) between 600 K and 723 K. At 773 K reduction to MoO_2 is observed. The same evolution of XRD powder patterns was measured during the thermal treatment of $H_3[PMo_{12}O_{40}]*13H_2O$ in 5 % H_2 in helium. This sequence of events coincides with the thermal analysis data (see Figure 5b) and identifies the cubic structure as the material responsible for selective oxidation activity.

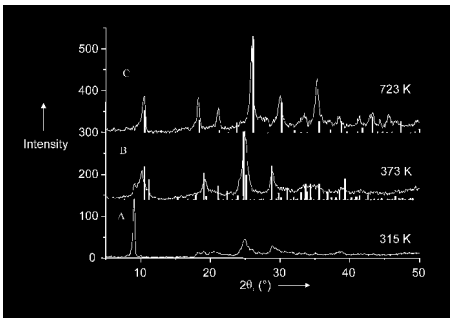

Fig. 10 X-ray diffraction patterns measured at selected temperatures during treatment of $H_3[PMo_{12}O_{40}]*13H_2O$ in 10% propene in helium. A) Pattern at 315 K corresponds to $H_3[PMo_{12}O_{40}]*8H_2O$ (no structural data available in the literature). B) Pattern at 373 K together with powder lines calculated for $H_3[PMo_{12}O_{40}]$. C) Pattern at 723 K together with powder lines calculated for $Cs_2H[PMo_{12}O_{40}]$.

In Figure 11 the XRD pattern of a cubic HPA obtained from $H_3[PMo_{12}O_{40}]*13H_2O$ after treatment in 10 % propene in helium (RT – 673 K) is depicted together with two simulated XRD powder patterns using two different structural models. The simulated XRD pattern in Figure 11A was calculated for a potassium salt of a molybdenum heteropoly acid ($K_2H[PMo_{12}O_{40}]*H_2O$, *Pn*-3*m*, [ICSD 209]). For the calculation the potassium ions were omitted and the cell parameter was adjusted to *a* = 11.853 Å. Although all peaks

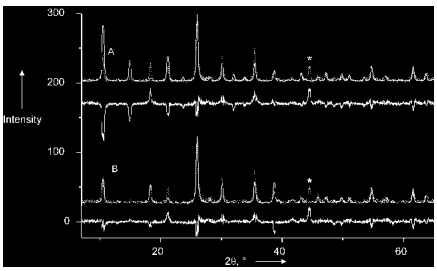

Fig. 11 Experimental XRD patterns of $H_3[PMo_{12}O_{40}]*13H_2O$ treated in 10% propene in the temperature range of 300 K - 673 K, (A) together with a calculated pattern of a "$H_3[PMo_{12}O_{40}]$" HPA based on structural data given in [ICSD 209] (*Pn*-3*m*, *a* = 11.853 Å), (B) together with a calculated pattern based on [ICSD209] with molybdenum at a cationic site. '*' indicates a reflection from the sample holder used. The differences between the experimental and the calculated patterns are also shown.

in the experimental pattern are accounted for by the cubic HPA phase and all peak positions agree well between experiment and calculation, a considerable deviation in the peak intensities of the two patterns can be seen. The simulated pattern in Figure 11B was calculated for a molybdenum heteropoly acid ([ICSD 209]) while a fraction of the molybdenum cations was placed on a cationic site outside the Keggin anion. The position of the cationic site (x=0.347; y=0.713; z=0.735), and the site occupancy factor (SOF) for this site (0.114) and for the molybdenum site in the Keggin anion (0.717) was refined by Rietveld analysis (WinMProf) [55]. The position of the other ions in the unit cell and the

site occupation factors (SOFs) for oxygen and for phosphorus were kept fixed in the refinement. Evidently, by placing a certain amount of molybdenum cations on sites outside the Keggin anions, the agreement between experimental data and simulated powder pattern is considerably improved. Thus, we propose that a cubic molybdenum autosalified HPA is formed from the triclinic free heteropoly acid during thermal treatment in 10 % propene. The lattice constant obtained for the cubic salified HPA (a = 11.853 Å) is very similar to that of the cesium salt of the heteropoly acid (a = 11.862 Å).

It cannot be ruled out that not a naked Mo^{6+} ion but molybdenyl species or reduced cations are taking the place of the alkali ion. There is no convincing way to determine the local charge distribution, as defects in the surrounding Keggin units have to be assumed. The XRD observations are not specific enough to validate the increase in structural complexity at the extra sites that will bring down further the intensity differences. A complementary local analysis is required to further substantiate autosalification.

In situ X-ray absorption spectroscopy

The evolution of the Fourier transformed Mo K edge χ(k) (pseudo radial distribution function, RDF) during thermal treatment of $H_3[PMo_{12}O_{40}]$*$13H_2O$ in 10 % propene is depicted in Figure 12A. The initial RDF can be very well simulated by theoretical calculations based on the structure of the undistorted Keggin anion. At ~ 400 K considerable changes in the first Mo – O coordination shell can be observed that indicate distortion compared to the initial Mo – O coordination in the Keggin anion. At ~ 600 K the entire RDF starts to change continuously into what can be assigned to the RDF of the molybdenum salified heteropoly acid (identified in used catalysts by XRD). Interestingly, the same evolution of RDF resulting in the RDF of a molybdenum salified heteropoly acid was observed during thermal treatment of $Cs_2H[PMo_{12}O_{40}]$ in 10 % propene. Conversely, no significant change in the local structure was detected during thermal treatment of $Cs_3[PMo_{12}O_{40}]$ under reducing conditions.

In Figure 12B, the Mo K edge-shift corresponding to the structural evolution depicted in Figure 12A is shown. At ~ 600 K strong reduction of the molybdenum in the heteropoly acid is observed that coincides with the formation of the molybdenum salified heteropoly acid (RDF in Figure 12A). From comparison with molybdenum oxide reference compounds [56] an average molybdenum valence of ~ 5.4 is estimated for the resulting molybdenum salified heteropoly acid.

In order to elucidate the short-range order structure of the molybdenum salified HPA, detailed XAFS analysis of the Mo K edge χ(k) was performed. Satisfying agreement between experimental data and theoretical XAFS calculations was achieved using the Mo – O and Mo – Mo distances and the respective coordination numbers in a Keggin anion as start parameters. This indicates, that to a certain degree the characteristic structure of the Keggin anion is preserved, however, with a considerably altered local geometric and

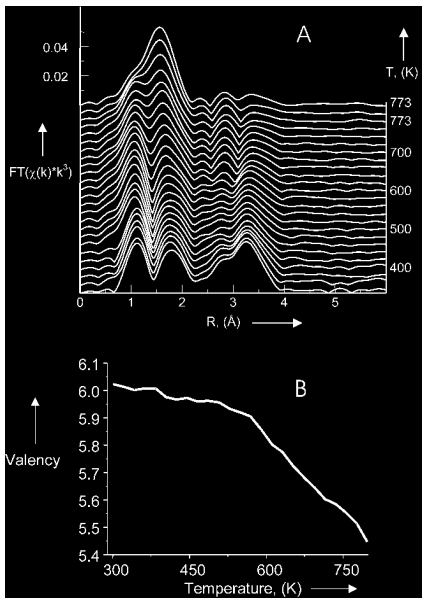

Fig. 12 (A) Evolution of Fourier transformed Mo K edge χ(k) measured during treatment of $H_3[PMo_{12}O_{40}]$*$13H_2O$ in 10% propene in helium in the temperature range of 300 K to 770 K. (B) Corresponding evolution of the average Mo valence as derived from the Mo K edge position.

electronic structure. Comparison of the theoretical and the experimental RDF of the molybdenum salified HPA together with the individual scattering paths in the RDF and the RDF of the free heteropoly acid and of ammonium heptamolybdate (AHM) is depicted in Figure 13. The RDF of

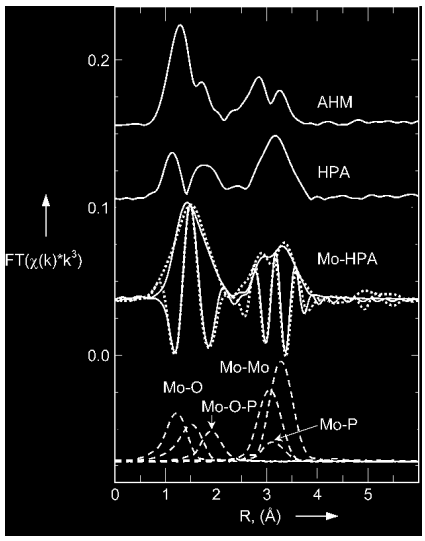

Fig. 13 Experimental Fourier transformed Mo K edge χ(k) of ammonium heptamolybdate (AHM), H3[PMo12O40]*13H2O (HPA), and the molybdenum salified HPA. For the latter, magnitude and imaginary part of a XAFS refinement based on the structure of the Keggin anion are shown. Individual scattering paths in the XAFS refinement are indicated.

the molybdenum salified HPA appears to resemble more closely that of AHM than that of the HPA. The increase in amplitude of the first Mo – O coordination sphere of Mo-HPA compared to HPA is because of a shift of the individual Mo – O shells and a resulting constructive interference of the corresponding XAFS χ(k) functions. The values of the Mo – O distances corroborate the analysis exhibiting a strong reduction in the Mo – O bond to the phosphate group of the Keggin anion. Furthermore, a reduction in the Mo – Mo distance in corner-sharing MoO_6 octahedra was observed, whereas the Mo – Mo distance in edge-sharing MoO_6 octahedra remains approximately the same.

For the Mo – O bond to the phosphate group in the center of the Keggin anion, a strongly reduced Debye-Waller factor is obtained for both the initial HPA and the molybdenum salified HPA. Moreover, taking the Mo – P bond into account in the theoretical XAFS calculations results in a significant improvement of the refinement. Hence, the medium range order resembles that of a Keggion anion. The lengthened Mo – O bond to the phosphate group of the Keggin anion may be indicative for a lacunary Keggin [10,57] structure with one or more MoO_6 units missing from the initial structure of the Keggin anion. Moreover, the detailed analysis of the local structure based on the Keggin anion structure is in good agreement with the analysis of the long-range order structure, which remains closely related to the cubic structure of a salified heteropoly acid composed of Keggin anions.

Table 1 reports the summary of characteristic structural parameters (coordination number (CN) and distance R of

Table 1: EXAFS structural parameters of the autosalified HPA (HPA*), of the parent free acid (HPA) and of model structures of a Keggin anion (KEG).

Pair	CN	R (HPA*)	σ (HPA*)	R (HPA)	σ (HPA)	R [KEG]
		(Å)	(Å^2)	(Å)	(Å^2)	(Å)
Mo-O	1	1.73	0.0035	1.69	0.0022	1.698
Mo-O	2	1.97	0.0025	1.83	0.0044	1.909
Mo-O	2	2.08	0.0015	1.99	0.0044	1.919
Mo-O-P	1	2.46	0.0010	2.43	0.0014	2.426
Mo-Mo	2	3.52	0.0020	3.41	0.0047	3.417
Mo-P	1	3.64	0.0009	3.57	0.0009	3.561
Mo-Mo	2	3.81	0.0032	3.71	0.0043	3.703

Mo – O and Mo – Mo coordination shells) of a Keggin anion model structure (based on [ICSD 209]) obtained from a refinement of the model structure to the experimental XAFS functions χ(k) of $H_3[PMo_{12}O_{40}]*13H_2O$ (HPA) and of the Mo salified HPA (HPA*) (N_{ind} = 25, N_{free} = 14, 7 single scattering paths and 5 multiple scattering paths) (E_0 (HPA*) = -3 eV, E_0 (HPA) = 1 eV).

Evidently, partially salified heteropoly acids composed of Keggin anions are not thermally stable at temperatures above ~ 600 K and under a reducing atmosphere. Under reaction conditions, a considerably modified local Mo coordination is observed together with a strongly altered electronic structure. The molybdenum salified HPA observed is formed by autosalification as a result of the migration of molybdenum cations from the Keggin to cationic sites in the HPA structure. It seems, that the changes detected in the local structure of the Keggin anions in the heteropoly acid result in the local geometric and electronic structure of the MoO_6 units that resembles that of hexavalent molybdenum in oligomeric molybdates. This change in the local geometric and electronic structure of the HPA under reaction conditions may be a prerequisite for the catalytic activity of heteropoly acids.

We propose that the same structural alterations observed (i.e. migration of Mo cations, partial reduction, modified short-range coordination) also take place under partial oxidation reaction conditions in both the free heteropoly acid and the cesium salt. This structural evolution under reducing conditions may be in agreement with a core-shell model under selective oxidation reaction conditions [26] where the cesium salt acts as nucleus coated by the molybdenum salified heteropoly acid. Because of the same lattice constant and structure, epitaxial orientation of the cesium salt and the molybdenum salified HPA should be feasible. From studies on the long-range order of the cesium salts of a HPA under reaction conditions, however, the formation of a molybdenum salified HPA will be very difficult to detect. Nevertheless, the characteristic changes in the short-range order reported here should be readily distinguishable.

The structural data give refined and more precise insights into the restructuring processes identified in the stability studies. After release of the crystal water the cationic voids

in the packing of the Keggin units become empty and allow the migration of some Mo cationic species into the secondary structure. Upon further thermal load the structural water is lost leaving behind a still three-dimensional M-O oligomer that exhibits significant relaxation of its local environment resembling more that of oligomolybdates than that of the distorted HPA precursor. Two new structures were identified that arrive from restructuring of the hydrated Keggin HPA and that are not amorphous precursors of the parent binary oxides. These oxides only occur at the end of the restructuring process and are irrelevant for good catalytic performance; the reverse synthesis of the HPA is the process of irreversible de-activation in catalysis. To re-activate or to inhibit this process choice of reaction conditions as closely as possible to the synthesis conditions is desirable; here is an explanation for the beneficial effect of a high partial pressure of steam in the feed allowing for local "hydrothermal" synthesis conditions. Such conditions will also relax the chemical stress on the oxides against reduction caused by the hydrocarbon components in the reaction mixture. Evidence from NEXAFS is presented that even without chemical stress the average electronic structure of the metastable intermediates is considerably different from the formal d^0 valence electronic configurations of cations constituting the parent Keggin structure. Evaluation of the redox states in the active states of the HPA is required.

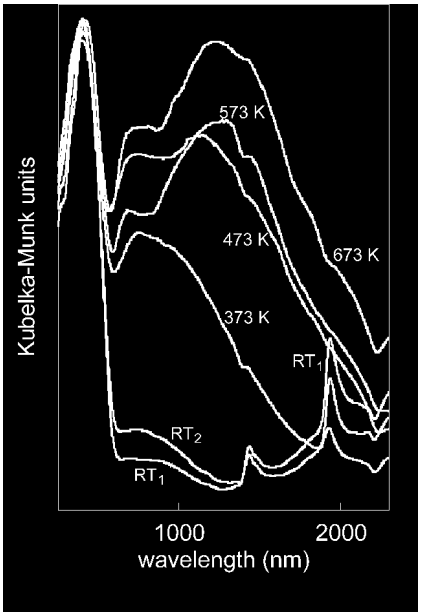

Fig. 14 In situ DR UV-Vis-near-IR spectra of $Cs_1H_3[PVMo_{11}O_{40}]$ from RT to 663 K. About 1 g of the HPA/SiO_2 mixture was filled into the cell; a He flow of 100 ml/min and a heating rate of 1 K/min were applied. Only selected spectra of the series are shown. The spectra RT_1 and RT_2 were obtained at 300 K with a drying He stream. The time elapsed between the two spectra was 2 h.

Electronic Structure by in situ UV-Vis-near-IR Spectroscopy

Summary of typical experimental results

For $CsH_3[PVMo_{11}O_{40}]*nH_2O$ treated in He from RT to 663 K the apparent absorption increases strongly with temperature as can be seen in Figure 14. Simultaneously, the near-IR absorption bands of the crystal water disappear completely. With increasing temperature broad absorptions develop first in the Vis spectral range and at higher temperatures also in the NIR region. Similar behaviour was observed for $H_4[PVMo_{11}O_{40}]*nH_2O$ and $Cs_2H_2[PVMo_{11}O_{40}]*nH_2O$ as shown and discussed in refs. [11,18,19]. Usually, the observed spectra are decomposed into Gauss profiles due to their strong broadening. This method is simple but quite arbitrary. Therefore, the first moment measuring the mean energy was evaluated in order to obtain more reliable information about the band evolution with increasing temperature and time on stream. The first moment is defined by the following equation:

$$\bar{\lambda} = \int_{\lambda 1}^{\lambda 2} \lambda * K(\lambda) d\lambda \; / \int_{\lambda 1}^{\lambda 2} K(\lambda) d\lambda \qquad (1)$$

Using Eq. (1) the first moments of the spectra acquired at different temperatures were obtained separately for the visible and near-IR spectral ranges. In these two cases the limits of integration have been chosen for the visible range from 500-580 nm(λ_1) to λ_2 = 840 nm. For the near-IR range these values are 870 nm and 2000 nm. For the visible range, the value λ_1 was varied to minimise overlap between the ligand-to-metal-charge-transfer (LMCT) absorptions and Vis bands arising mainly from intra-atomic d-d-transitions and metal-metal charge transfer. For the full spectra the mean energy can be written as:

$$\bar{\lambda} = \left(\int_{\lambda 1}^{840} \lambda * K(\lambda) d\lambda + \int_{870}^{2000} \lambda * K(\lambda) d\lambda \right) / \left(\int_{\lambda 1}^{840} K(\lambda) d\lambda + \int_{870}^{2000} K(\lambda) d\lambda \right) \qquad (2)$$

where λ_1 = 500-580 nm.

The resulting values as function of temperature for the two spectral ranges as well as for the whole spectrum are reported in Figure 15A for the free acid $H_4[PVMo_{11}O_{40}]*nH_2O$ and in Figure 15B for $CsH_3[PVMo_{11}O_{40}]*nH_2O$. The Vis part shifts barely with temperature for the $H_4[PVMo_{11}O_{40}]*nH_2O$, but it moves considerably for the salt whereas the inverse situation occurs for the near-IR band. The strong contribution of the near-IR band determines the different sensitivity of the whole spectrum to these changes. This result reveals the value of advanced positional analysis that shows the different origins for the phenomenologically same band shifts in the two materials.

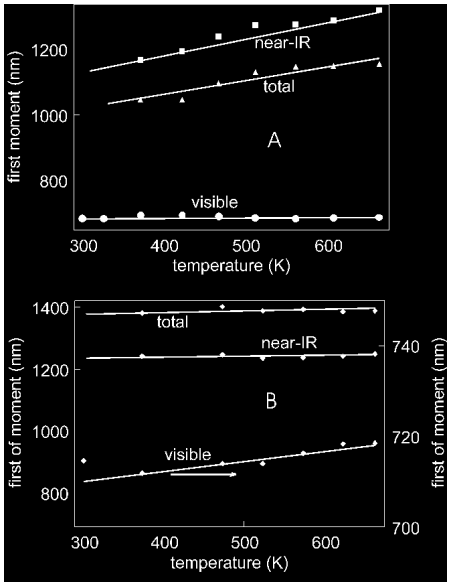

Fig. 15 Panel (A): Temperature dependence of the first moment of the visible, near-IR and total spectra of $H_4[PVMo_{11}O_{40}]$ in a He stream. Panel (B): First moment of the visible, near-IR and total spectra of $CsH_3[PVMo_{11}O_{40}]$ as a function of temperature in a He stream.

Data analysis using semi-empirical theory

The apparent absorption bands in HPA and its salts originate from d-d transitions in reduced V and Mo ions and from inter-valence-charge-transfer (IVCT) bands. These bands designate binuclear metal centers bridged by at least one oxygen atom in which the formal oxidation states are d^0 and d^n for the metals. The shape and the intensity of the IVCT bands are determined by vibrational coupling parameters and by parameters characterizing the electron transfer between different metal sites of the Keggin molecule [11,19]. As the intensity of an IVCT transition is proportional to the square of the electron transfer parameter, the most intense charge transfer bands arise from the transitions in which the only one d^1 electron is excited from its original site to a neighboring one. Therefore, while calculating the absorption spectrum of a reduced Keggin unit we only take into account single-electron transfers between adjacent edge-sharing and corner-sharing metal sites. IVCT transitions in the visible and near-IR range occur from the transfer of an excess electron (chemically situated at Mo^{5+} or V^{4+} sites) between the ground states of neighbouring metal centers. While calculating the transfer and vibrational coupling parameters, the distances between the ions in MO_6 units as well as between different units are taken close to those in HPA. Microscopic estimations testify [11] that the transfer parameters are small in comparison with the vibrational coupling constants for the ground states. This allows us to reduce the problem of calculating the IVCT band positions of the whole Keggin unit (intact or defective) to the problem of light-induced electron transfer between two adjacent metal ions (Mo^{5+}, Mo^{6+} or V^{4+}, Mo^{6+}). The geometric structure of reduced binuclear mixed-valence species responsible for the spectral transformations on different stages of the experiment will be denoted as

$((O_t)_{1-s_i}(O_p)_{1-y_i}(O_b)_{3-x_i}H_{\alpha z_i})d^1$-$O_b$-$d^0((O_t)_{1-s_j}(O_p)_{1-y_j}(O_b)_{3-x_j}H_{\beta z_j})$,

where d^1 designates the 3d or 4d electron, O_b, O_t are the bridging and terminal oxygens, O_p stands for the oxygen in the phosphorus tetrahedral environment, s_i, x_i and y_i are the numbers of oxygen ions extracted in the process of constitutional water or oxygen evolution, z_i is the number of protons localized on the moiety, and α=b or t for protons residing on the oxygen species O_b and O_t, respectively. The composition of very likely species was chosen on the basis of TG, DSC and IMR-MS analysis [11] and using the information presented in Figures 1-5. Spectral parameters were derived from studies of MoO_3 [11,58,59]. For sampling of species with the most probable number of localized protons or oxygen vacancies the methods of probability theory [60] have also been applied.

The temperature dependence of the maxima of charge-transfer bands arising from intact and defective binuclear species is displayed in Figure 16. Two main effects can be noticed analyzing the curves. Firstly, reduced binuclear species $M_2O_{11}H_b$ (M-metal ion) with protons localized on the bridging oxygen atoms (O_b) give blue shifted charge transfer bands relative to those arising from intact ones M_2O_{11} (compare curves 7, 9, 13 for V^{4+}-Mo^{6+} and 17, 18, 20 for Mo^{5+}-Mo^{6+} in Fig. 16). Secondly, the removal of bridging oxygen (species M_2O_{10}) clearly results in a further blue shift in the

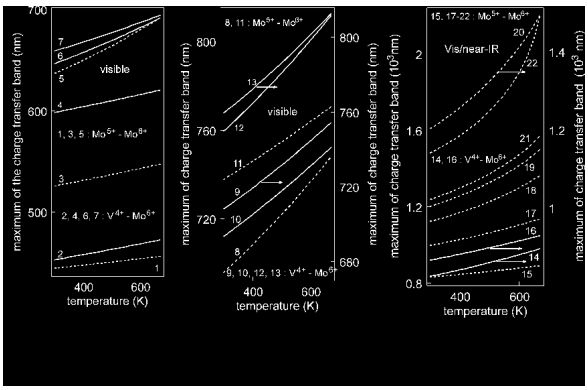

Fig. 16 Summary of semi-empirical calculations for the temperature dependence of the peak positions of the charge transfer bands arising from $((O_t)_{1-s1}(O_p)_{1-y1}(O_b)_{3-x1}H\alpha_{z1})d^1$-$O_b$-$d^0((O_t)_{1-s2}$- $(O_p)_{1-y2}$ $(O_b)_{3-x2}H\beta_{z2})$ species. 2, 4, 6, 7, 9, 10, 12, 13, 14, 16 - V^{4+}-Mo^{6+}, 1, 3, 5, 8 , 11, 15, 17-22 - Mo^{5+}-Mo^{6+},1. s_i=y_1 =x_2 = z_i =0, x_1 =y_2 =1; 2, 5. s_i =y_i =z_i=0, x_i =1; 3, 6. s_i =y_i =z_i =x_2=0, x_1 =1; 4, 15.s_i =y_1 =x_i =z_i =0, y_2 =1; 7, 14, 17. s_i =y_i =x_i =z_2 =0, z_1 =1, α=b; 8. s_i =y_2 =x_2 = z_i =0, y_1 =1, x_1 =1; 9, 18. s_i =y_i =x_i =0, z_i =1, α,β=b; 10, 21. y_i =x_i =z_i=0, s_i =1; 11. s_i =y_i =x_i = z_1= 0, z_2 =1, β=t; 12, 19. s_1 =y_i =x_i =z_i =0, s_2=1; 13, 20. s_i =y_i =x_i =z_i =0; 16, 22. s_i =x_i =z_i =0, y_i =1; For explanation of the symbols see text and ref. 11.

transition energy (curves 3 and 17). These results obtained allow qualitative explanation for the change in the mean energy for HPA and its salts in the temperature range RT-663 K under helium flux (Fig. 15). Nearly all d-d transitions in the range $\lambda > 400$ nm contribute to the visible part of the spectra (transitions with smaller wavelengths $\lambda < 400$ nm are not considered because they overlap with the LMCT). Besides the d-d transitions a large number of intervalent transitions of the type of

Mo^{5+}-O_b-Mo^{6+} → Mo^{6+}-O_b-Mo^{5+}
V^{4+}-O_b-Mo^{6+} → V^{5+}-O_b-Mo^{5+}

also occur this spectral range.

Analysis of the thermal behaviour of HPA

At 300 K the loss of crystal water begins after a certain time of gas flux in $H_4[PVMo_{11}O_{40}]*nH_2O$ [11] and $CsH_3[PVMo_{11}O_{40}]*nH_2O$ (Fig. 2 and 14). At this initial stage there is no reduction, the $H_4[PVMo_{11}O_{40}]*nH_2O$ and $CsH_3[PVMo_{11}O_{40}]*nH_2O$ are partially hydrated, and the protons are not localized and reside on the bridging water moieties $H_5O_2^+$. Thus initially, the spectra should originate from the d-d transitions in the V^{4+} and Mo^{5+} ions and the charge-transfer bands arising from reduced $VMoO_{11}$ and Mo_2O_{11} species (Fig. 16, curves 13 and 20). Nevertheless, the intensity of the charge-transfer band induced by intervalent transitions in Mo_2O_{11} clusters at 300 K is lower than that of the band given by $VMoO_{11}$ clusters. The minimum of the adiabatic ground state corresponding to the excess electron localized on the V site lies considerably lower than that for the excess electron localized on a Mo site. At the same time the d-d transitions yield a much more intense band in the visible spectral range at 300 K than the charge-transfer band from species $VMoO_{11}$. In the hydrated phase the electron transfer is noticeably suppressed due to the high value of the dielectric constant reducing the Coulomb interaction between metal sites facilitating this transfer. Thus we can conclude that at about 300 K the visible spectral range mainly originates from the d-d transitions in V^{4+} and Mo^{5+} ions.

With the rise of temperature the crystal water evolves, and the total intensity of the spectra from $CsH_3[PVMo_{11}O_{40}]*nH_2O$ and from $H_4[PVMo_{11}O_{40}]*nH_2O$ increases due to a rising contribution from the charge-transfer bands. The reason for this is that with water removal the screening of the electrostatic interaction between the metal ions is lifted, the dielectric constant ε goes down and consequently the transfer parameters increase.

At temperatures from 326 K to 422 K the loss of crystal water is accompanied by the localization of acidic protons, the most preferable sites of which are the bridging oxygen ions. The resulting species $MO_6(H_b)$ ($M=V^{4+}$, Mo^{5+}) displays three d-d bands in the visible range. These transitions are higher in energy than the corresponding transitions in intact MO_6 ($M=V^{4+}$, Mo^{5+}) species. In addition, two new binuclear species $(VH_b)MoO_{11}$ (for brevity, we denote the metal ion in whose nearest surrounding a proton resides by MH_b), (VH_b)-$(MoH_b)O_{11}$ (Fig. 16, curves 7, 9) exhibit IVCT transitions at shorter wavelengths (compare 666 nm, 717 nm, for $(VH_b)MoO_{11}$, $(VH_b)(MoH_b)O_{11}$ and 770 nm for $VMoO_{11}$ Fig. 16, curve 13 at 380 K). The reduced less probable $Mo_2O_{11}H_t$ cluster and the cluster $V(MoH_b)O_{11}$ also yield IVCT transitions in the Vis spectra part (Fig. 16, curves 11 and 14). Thus, at temperatures between 326 K and 422 K, the Vis part of the charge transfer band is formed by IVCT transitions in intact and protonated V^{4+}-Mo^{6+} species. In reduced species $(VH_b)MoO_{11}$, $(VH_b)(MoH_b)O_{11}$, $VMoO_{11}$ the positions of the IVCT transitions shift insignificantly in this temperature range as can be seen in Fig. 16. For instance, the peak positions of the IVCT transition in the $(VH_b)MoO_{11}$ cluster are 661 and 670 nm at temperatures 330 and 420 K, respectively. Using probability theory [60], it can be shown for $H_4[PVMo_{11}O_{40}]$ that at 422 K, when crystal water is removed, the number of Keggin anions with four acidic protons located only on Mo ions is twice as large as compared to the number of anions with protons distributed between one V ion (1 proton) and 11 Mo ions (3 protons). Consequently, the number of the IVCT transitions V^{4+}-Mo^{6+} between neighboring V and Mo ions in species $(VH_b)MoO_{11}$, $(VH_b)(MoH_b)O_{11}$ is small due to the Keggin structure (11 Mo sites at least per polyanion). In addition, the maximum number of d-d transitions from protonated units is 28 per Keggin anion at 422 K for HPA [11] instead of 24 for an undamaged anion. In consequence, for $H_4[PVMo_{11}O_{40}]$ the mean energy (first moment) of the Vis spectral part remains practically unchanged in the range 373-422 K, as shown by experiment (Fig. 15A). The high-energy edge of the visible range shifts to higher values. The spectral intensity at these energies is, however, insignificant and does not affect the first moment of the Vis band.

The situation is quite similar for $CsH_3[PVMo_{11}O_{40}]$ in the range of crystal water removal. It is pointed out that the values of the mean energies are higher in $CsH_3[PVMo_{11}O_{40}]$ due to the stronger crystal field and the enhanced coupling between electronic and vibrational states caused by the rigid filling of the secondary structure with Cs ions.

As the temperature continues to rise above 423 K, structural water evolves (see TG data in [11]). This water is formed by the extraction of oxygen by two protons and leads to the formation of defective clusters in which bridging oxygen ions are removed. However, the evolution of structural water is experimentally not accompanied by the appearance of new reduced clusters. Therefore, the initial transformation of the visible spectral region has to occur from the dehydration of reduced species of the type of $VMoO_{10}$, Mo_2O_{10}, $VMoO_9$, Mo_2O_9 (Fig. 16, curves 1-6, 8, 10) and indicates the protonation of these reduced species. It cannot be excluded that the evolution of molecular oxygen from intact non-reduced $VMoO_{11}$, Mo_2O_{11} moieties [3] could also lead to the above-mentioned reduced fragments. However, in the temperature range 420-670 K the peak positions of the charge transfer bands from species

$(O_tO_p(O_b)_2)Mo^{5+}$-O_b-$Mo^{6+}(O_t(O_b)_3)$,
$(O_tO_p(O_b)_2)$-V^{4+}-O_b-$Mo^{6+}(O_tO_p(O_b)_2)$,

$(O_tO_p(O_b)_2)Mo^{5+}$-O_b-$Mo^{6+}(O_tO_p(O_b)_3)$
(Fig. 16, curves 1-3) fall inside the ranges 448-456 nm, 458-472 nm and 532-547 nm, respectively. These positions overlap with the LMCT band and cannot be singled out. Therefore, their contribution to the first moment is not accounted for within the limit for the Vis range.
Other binuclear metal-oxo species exhibiting oxygen defects (Fig. 16, curves 4-6, 8, 10) exhibit characteristic transitions within the window of observation of Figure 15. Likely geometric structures of such species are
$(O_tO_p(O_b)_3)V^{4+}$-O_b-$Mo^{6+}(O_t(O_b)_3)$,
$(O_tO_p(O_b)_2)Mo^{5+}$-O_b-$V^{5+}(O_tO_p$-$(O_b)_3)$,
$(O_t(O_b)_2)Mo^{5+}$-O_b-$Mo^{6+}(O_tO_p(O_b)_3)$.
Their relevant band positions are depicted in Fig. 16, curves 4-6, 8, 10. At temperatures from 420-670 K their IVCT transitions lie in the ranges 605-620 nm, 660-691 nm, and 710-747 nm, respectively, while the IVCT transition in the intact reduced cluster $VMoO_{11}$ shifts from 775 to 812 nm. The number of species with oxygen vacancies giving IVCT transitions in the visible range is expected to be much smaller than that of intact clusters as no extra feature appears in the expected spectral window. Therefore, at higher temperatures only an insignificant shift in the mean energy of the Vis spectral part is observed (see Figure 15) for $H_4[PVMo_{11}O_{40}]$ and $CsH_3[PVMo_{11}O_{40}]$. The cancellation of two effects of the formation of lacunary and reduced species is responsible for the only apparent insensitivity of the optical spectra to the dynamic transformations. This finding explains the apparent contradiction between structural studies revealing the dynamic behaviour found initially in the thermal analysis data and by optical spectroscopy. It is of utmost importance that this analysis corroborates the formation of defective M-O clusters still within the superstructure of lacunary Keggin ions. The analysis further reveals that these species are a minority fraction of all cluster anions. These defective fragments may thus be good candidates for the active sites in catalysis.
One main trend can be identified in the temperature behaviour of the near-IR spectra for $H_4[PVMo_{11}O_{40}]$*nH_2O. The first near-IR band originates at 300 K from the homonuclear intervalence transition
Mo^{5+}-Ob-Mo^{6+} → Mo^{6+}-Ob-Mo^{5+}
in intact Mo_2O_{11} species (model for reduced triads in the Keggin motif). The intensity of the near-IR spectral range is lower than that of the Vis part. Between 326 K to 420 K the crystal water is removed and the contributions to the near-IR band arise from the same homonuclear
Mo^{5+}-Ob-Mo^{6+} → Mo^{6+}-Ob-Mo^{5+}
intervalence transitions in reduced intact and protonated species of the type of
$(O_tOp(O_b)_3)Mo^{5+}$-O_b-$Mo^{6+}(O_tO_p(O_b)_3)$,
$(O_tOp(O_b)_3H_b)Mo^{5+}$-O_b-$Mo^{6+}(O_tO_p(O_b)_3)$,
$(O_tO_p(O_b)_3H_b)Mo^{5+}$-$O_b$-$Mo^{6+}(O_tO_p(O_b)_3H_b)$
(Fig. 16, curves 20, 17 and 18). The maxima of the charge transfer bands arising from species with acidic protons localized on bridging oxygen sites (Fig.16, curves 17, 18) are blue-shifted in comparison with those arising from Mo_2O_{11} species. In spite of this, the first moment of the observed near-IR spectral part (Fig. 15) for $H_4PVMo_{11}O_{40}$ exhibits a red-shift in the temperature range 371-422 K. This is again due to varying spectral weights of the different contributions. The relative spectral weights of reduced species Mo_2O_{11}, $(MoH_b)MoO_{11}$ and $(MoH_b)(MoH_b)O_{11}$ to the full spectra were found to be 18%, 33% and 13%, respectively. Consequently, the total contribution from species Mo_2O_{11} and of $(MoH_b)(MoH_b)O_{11}$ is of the same weight as for species $(MoH_b)MoO_{11}$. At temperatures of 370 K and 420 K the protonated species (Fig. 16, curves 17, 18) enumerated above exhibit peak positions at 1020 nm, 1036 nm, 1156 nm and 1182 nm, while at the same temperatures in the intact reduced species the charge transfer band exhibit maxima at 1241 nm and 1271 nm (Fig. 16, curve 20). These weighted contributions explain the observed red shift of the first moment of the near-IR band. Due to the smaller number of protons in $CsH_3[PVMo_{11}O_{40}]$ the red shift of the near-IR spectra part is less pronounced in this compound.
At higher temperatures the formation of defects also has consequences on the NIR spectral part. The newly appeared reduced, protonated species, for instance of the type of
$(O_p(O_b)_3)Mo^{5+}$-O_b-$Mo^{6+}(O_p(O_b)_3)$,
$(O_t(O_b)_3H_b)Mo^{5+}$-O_b-$Mo^{6+}(O_t(O_b)_3H_b)$
(Fig. 16, curves 21 and 22) exhibit IVCT transitions and several d-d transitions in the interval 1240-2200 nm. This explains the growth of the near-IR band to the low energy side at high temperatures. At the same time species of the type of
$(O_tO_p(O_b)_3)Mo^{5+}$-O_b- $Mo^{6+}(O_t(O_b)_3)$,
$(O_t(O_b)_3)V^{4+}$-O_b-$Mo^{6+}(O_t(O_b)_3)$
(Fig. 16, curves 15 and 16) with vacancies in the Op positions exhibit intervalence transitions that fall in the range of 860-930 nm at temperatures between 500-670 K. The lacunary species that appear in the process of the decomposition of the Keggin structure cause the observed increase in the intensity of the near-IR band as well as the expansion of the wavelength range in which this band occurs. As a result, the mean energy of the near-IR band continuously shifts to the red (Fig. 15).
The in-depth analysis of shape and dynamics of the optical spectra thus have brought about not only yet another independent confirmation of the catalytic relevance of oligomeric defective but still superstructured oxo-clusters. In addition detailed structural prototypes requiring as minimum complexity binuclear clusters with defects, chemical reduction and protonation as independent secondary variables were derived from the analysis of the two-dimensional information of spectral weight (position time intensity) versus sample temperature. It became evident that a sample with homogeneous geometric structure is by no means homogeneous at the molecular level. As none of the methods applied so far are truly surface-sensitive there is no information available about the lateral and in-depth distribution of these sites representing on average a cubic packing of Keggin motif.
The function of the HPA systems in selective oxidation phenomenologically requires the presence of strongly acidic

sites that are believed to enable C-H bond activation. In the Introduction it was said that the determination of the acidity of the activated HPA is a non-trivial problem. Thus it is of great relevance to find a sign of acidity as otherwise no solid proof exists for the bifunctional character of HPA. It may well be argued that the acidity of HPA precatalysts is a secondary property over the Keggin structural motif that is clearly required as superstructure for the active sites characterised so far.

Acid-Base Properties under Relevant Conditions

A family of heteropoly compounds comprising the acids $H_{3+x}PMo_{12-x}V_xO_{40}$ with x = 0-2 and the corresponding salts with partial or complete replacement of the protons by cesium was investigated by adsorption of probes that presumably will not form salts. This usually overlooked deficiency of "typical" acid probes such as ammonia or pyridine hampers previous investigations the same way as the redox-labile character of the probe molecules that tend to reduce HPA. Carbon monoxide was selected because it is an excellent probe for Brønsted and Lewis acid sites [61]. IR spectroscopy was chosen as the method of analysis, because unlike calorimetry or TPD, it gives information on the nature of the sites and with the right probes is fairly sensitive to small energetic differences between sites. IR spectroscopy has been applied extensively for the structural characterization of heteropoly compounds at various temperatures and degrees of dehydration [62,63,64,65,66,67,68,69]. This method in addition delivers information on the structure of a sample after each treatment by investigating the low-frequency range of the IR spectrum.

Thermal Stability of HPA seen by IR

Transmittance through the acids (no Cs) was poor and CO adsorption could not be observed. After activation at 523 K, the samples $Cs_xH_{4-x}PVMo_{11}O_{40}$ (x=2-4) displayed a broad band at 4050 cm^{-1} and a band at 3445 cm^{-1} with a shoulder at approximately 3285 cm^{-1}. The intensity of the shoulder decreased from x = 2 to x =3, i.e. with increasing Cs content. A weak, narrow band at 3535 cm^{-1} was observed for $Cs_xH_{4-x}PVMo_{11}O_{40}$ with x = 2-4. After treatment at 673 K, $Cs_4PVMo_{12}O_{40}$ was devoid of any OH groups, and the spectra of $Cs_3HPVMo_{12}O_{40}$ and $Cs_2H_2PVMo_{12}O_{40}$ were similar in the OH region with a slightly asymmetric band centered at about 3425 cm^{-1}. The band at 4050 cm^{-1} disappeared with the treatment at 673 K. The spectrum of $Cs_2HPMo_{12}O_{40}$ treated at 523 K showed two overlapping bands at approximately 3380 and 3240 cm^{-1}. Both bands were weakened after treatment at 673 K and better separated with positions at 3390 and 3230 cm^{-1}.

Overtones and combination modes of metal- and phosphorus-oxygen vibrations were observed in the range of 2150–1850 cm^{-1}. The spectrum of $H_3PMo_{12}O_{40}$ exhibited one strong band at 1985 cm^{-1} and a number of ill-defined and weak bands. Three strong bands at 2165, 2130, and 1990 cm^{-1} and one weak band at 2040 cm^{-1} characterized the spectrum of $H_4PVMo_{11}O_{40}$. For $Cs_xH_{4-x}PVMo_{11}O_{40}$ (x=2–4) three intense bands were found at 2120 cm^{-1} (s, sh towards higher wavenumbers), 2035 cm^{-1} (s, sh towards higher wavenumbers), and 1935 cm^{-1} (vs, sh towards higher and lower wavenumbers). Depending on the Cs content and the treatment the position of the band varied by ±5 cm^{-1}. The general trend was a shift towards higher wavenumbers with increasing treatment temperature. The spectra of $Cs_2HPMo_{12}O_{40}$ also showed strong bands at similar positions as the other Cs-salts, namely at 2124, 2040, and 1941 cm^{-1}. Instead of shoulders towards higher wavenumbers on the bands at 2040 and 1941 cm^{-1}, two bands at 2057 and 1975 cm^{-1} were clearly separated. All of these bands remained unchanged within the detection limits during CO adsorption.

The first harmonics of the metal- and phosphorus-oxygen vibrations were not accessible in transmission mode because of the cut-off of the CaF_2 windows.

These data confirm that thermal treatment modifies the oxo anions but does not lead to expulsion of the central heteroatom and hence preserves the Keggin motif. These findings are in qualitative agreement with all other evidences presented here and indicate that thermal treatment alone without chemical reductive stress does not lead to a complete breakdown of the HPA structure. The loss of –OH groups of all partly salified samples between 573 K and 673 K is a good indication for the similarity of the present sample preparation to the in situ structure-sensitive experiments described above. This result questions the statement about the relevance of Brønsted acidity (acid protons) for the catalytic process that sets in concomitantly with the loss of the –OH groups (compare with Figure 5b).

Analysis of CO adsorption data

Representative spectra obtained during CO adsorption following activation at 523 and 673 K are shown in Figure 17.

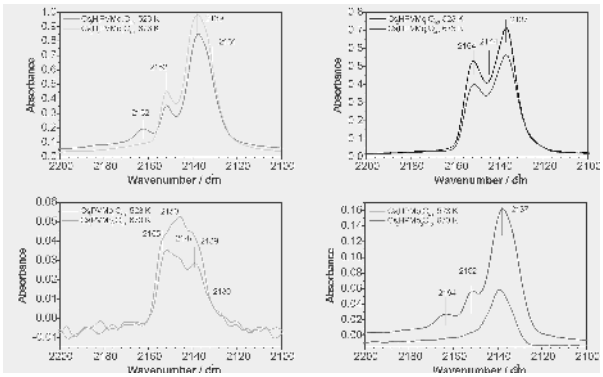

Fig. 17 FTIR spectra, difference of spectra of the sample in presence of CO / in vacuum; recorded at 77 K in transmission with self-supporting wafer. Top left: $Cs_2H_2PVMo_{11}O_{40}$; activation at 523 K: $p_{CO} = 5.2*10^{-1}$ hPa; activation at 673 K: $p_{CO} = 2.8*10^{-1}$ hPa. Top right: $Cs_3HPVMo_{11}O_{40}$; activation at 523 K: $p_{CO} = 3.2*10^{-1}$ hPa; activation at 673 K: $p_{CO} = 3.5*10^{-1}$ hPa. Bottom left: $Cs_4PVMo_{11}O_{40}$; activation at 523 K: $p_{CO} = 2.26$ hPa; activation at 673 K: $p_{CO} = 2.9*10^{-1}$ hPa. Bottom right: $Cs_2HPMo_{12}O_{40}$; activation at 523 K: $p_{CO} = 7.1*10^{-1}$ hPa; activation at 673 K: $p_{CO} = 3.3*10^{-1}$ hPa. Pressures were selected to represent spectra of similar intensity.

At equal partial pressures, the band intensities were roughly proportional to the surface area of the samples. The best spectra were thus obtained for $Cs_2H_2PVMo_{11}O_{40}$ and $Cs_3HPVMo_{11}O_{40}$. Often, broad features of overlapping bands were observed. Series of spectra in dependence of the CO partial pressure were thus evaluated and also fit in order to identify all bands. The band positions are given in Table 2.

Table 2: IR band positions of CO absorption frequencies for several HPA samples activated at the temperatures given.

Sample and activation	Band positions in cm^{-1}
$Cs_2H_2PVMo_{11}O_{40}$, 523 K	2162 2152 2139 2131
$Cs_2H_2PVMo_{11}O_{40}$, 673 K	2152 2139 2132
$Cs_3HPVMo_{11}O_{40}$, 523 K	2154 2147 2137
$Cs_3HPVMo_{11}O_{40}$, 673 K	2154 2144 2137
$Cs_4PVMo_{11}O_{40}$, 523 K	2153 2147 2139 2130
$Cs_4PVMo_{11}O_{40}$, 673 K	2155 2150 2145 2140 2135
$Cs_2HPMo_{12}O_{40}$, 523 K	2164 2152 2137 (very broad)
$Cs_2HPMo_{12}O_{40}$, 673 K	2153 2139 (very broad)

According to the literature [48] the band at 2162-2164 cm^{-1} can be assigned to CO adsorbed on OH groups. The best evidence of CO adsorption on OH groups is a shift of the OH band parallel to the development of the corresponding CO band; no such shift was observed in our case. Other arguments though suggest adsorption of CO on OH groups: (i) the band position is typical of OH-coordinated CO, (ii) the band is observable after treatment at 523 K but not after treatment at 673 K, it is consistent with dehydroxylation, and (iii) the band is not observed for the Cs-rich and thus H-poor compounds. It appears that the shift of the OH groups could not be observed because the quality of the spectra in this range is poor and/or only a fraction of the OH groups is acidic enough for interaction.

The band at 2152-2155 cm^{-1} has been assigned previously [48] to the adsorption of CO on Cs. This band, which was typically rather narrow, was found for all Cs-containing samples and the relative intensity increased with increasing Cs content.

It has been suggested that the band at 2137-2140 cm^{-1} arises from "physisorbed or liquid-like CO" [48]. Not always but frequently are such bands only formed at high CO coverage, and Saito et al. [48] fitted the band with a Lorentzian line profile. We detected this band already at CO pressures $<10^{-3}$ hPa, and the line profile was not Lorentzian. However, as we observed this band for all samples, it might indeed be unspecific adsorption, not meriting further interpretation at the current state of investigation.

Most interesting are two additional bands that were not reported before: the band at 2144-2147 cm^{-1}, which is present in the spectra of $Cs_3HPVMo_{11}O_{40}$ and $Cs_4PVMo_{11}O_{40}$, and the band at 2130-2135 cm^{-1}, which is present in the spectra of $Cs_2H_2PVMo_{11}O_{40}$ and $Cs_4PVMo_{11}O_{40}$. Besides the OH-groups and Cs cations, other sites may also interact with the CO. Lewis acid sites could be created by defects (oxygen vacancies) in the Keggin units of the heteropoly compounds or through fragmentation of Keggin units. Coordinatively unsaturated Mo or V cations could represent such Lewis sites. Single bands at these positions are not typical of CO adsorption on Mo cations. Only bands in band pairs, indicating geminal CO species at Mo^{4+} and Mo^{2+} species, respectively, have been reported at these positions [70]. Neither did we observe band pairs nor are Mo^{2+} species expected, because XPS measurements [71] have shown that, e.g., Mo in $H_3PMo_{12}O_{40}$ is reduced to Mo(IV) only through extensive treatment in H_2 at 623 – 673 K and under milder reduction conditions remains Mo(VI) or becomes Mo(V). We generated reference data by adsorbing CO on mechanically activated MoO_3 and V_2O_5. Among the features observed for both compounds were bands at ca. 2145 and 2130 cm^{-1}, indicating that these band positions are possible for CO adsorbed as well on Mo as on V cations. The two bands observed for various heteropoly compounds can thus be assigned to coordinatively unsaturated metal cations, i.e. Lewis acid sites; but neither of the two bands is characteristic of a particular metal cation. Most likely, the cations are reduced with respect to the original oxidation state, and the band with the lower frequency represents less positively charged species and thus a softer Lewis acid.

No assignment can be made yet for the band at 2150 cm^{-1}, which appears only in the spectra of $Cs_4PVMo_{11}O_{40}$.

As mentioned before, the intensity of the CO bands depends roughly on the BET surface area of the sample, suggesting that CO interacts only with the surface. The bands representing the overtones and combination modes of the metal- and phosphorus oxygen vibrations did not change upon CO adsorption. Either only a small surface fraction of the sites interacts and the changes are below detection limit, or these bands represent only intact Keggin units, which do not interact with CO.

The following picture evolves from our experiments: the stability of $Cs_3HPVMo_{11}O_{40}$ is also manifested in the CO

adsorption data; it is the only compound that yields the same CO band pattern after activation at 523 K and 673 K. All other samples undergo significant changes when heated to the higher temperature. The Mo/V cations in $Cs_3HPVMo_{11}O_{40}$ are also not reduced as much by the activation procedure as in $Cs_2H_2PVMo_{11}O_{40}$ and $Cs_4PVMo_{11}O_{40}$. The investigated heteropoly compounds provide more surface sites than just OH-groups and Cs cations, i.e. different types of Lewis sites. The observation of such sites is consistent with the partial decomposition of the Keggin units.

The probe molecule adsorption study was intended to discuss the presence of –OH groups on activated samples. The main result was, however, the detection of adsorption sites developing only after activation of the HPA that were not described earlier as other studies addressed the chemisorption properties of the parent HPA. It may be speculated that only the reduced species of lacunary Keggin units that were identified by DRS spectroscopy and that contribute to the Mo K-edge NEXAFS shift produce sites that adsorb CO at 2130 cm^{-1}. These sites are redox active and may be able to provide enough electrons (two electrons per molecule and site) to bind and cleave molecular oxygen. These sites are not unique to V-substituted HPA as the band at 2130cm^{-1} may also be present in $Cs_2HPMo_{12}O_{40}$.

Conlusions

The set of complementary in situ studies focused on one family of molybdenum-based HPA has produced clear evidence that neither the parent Keggin ions nor their perfect salt crystals are the catalytically active phase. Already in water the ionic crystals dissolve and the Keggin ions deprived of their stabilizing secondary structure hydrolyze and set free their templating central heteroatom.

In gas-phase reactions activity sets in abruptly after, again, the removal of the secondary structure by evaporation of water or decomposition of counterions. If the secondary structure is completely non-volatile (fully salified) then no catalytic activity is observed at all.

The loss of the secondary structure is connected to the formation of defective void structures of the Keggin ion (lacunary species). If these species are partially reduced and exhibit sites of substantial local electron density, then they may behave as active sites for redox catalysis.

The openings in the Keggin ions may not grow above a critical size. Then, under the action of either water or reducing gas-phase species the central templating heteroatom is lost as phosphate or PH_3. The presence of this template is vital for the function of the catalyst as was also shown by replacing P by Si which is much less stable. In the absence of the template the molybdate species restructure into fragments of binary oxides that are “at best” active in total oxidation catalysis (concept of site isolation in selective oxidation).

The vital hindrance of falling apart of the defective Keggin units is kinetically supported by the presence of a non-volatile secondary network of ions of alkali or low-valent transition metal species. Its abundance should be sufficient to link all defective Keggin units but must not block all empty space between the Keggin units in order to allow the defect formation associated with the expulsion of Mo-species. These Mo species also fulfill the function of a salifying species in the absence of other non-volatile cations. This is the case in “free acid” catalysts that are highly active and selective but also highly unstable. This instability is the expression of the insufficient adaptation of the charge-to-radius ratio for Mo-cations as compared with Cs (concept of hard and soft Lewis acid-base reactions).

These findings explain the critical character of the HPA in catalysis. Their active states are highly metastable intermediates in the destruction process of a superstructure (Keggin crystal) that is only stable with a complete secondary structure giving no space for the Keggin anions to fall apart. The two independent variables determining the metastability are the extent and local distribution of the secondary structure and the partial pressure of reducing species removing the central templating heteroatoms. As under reaction conditions the defective crystals were shown to behave dynamically and restructure in core-shell distributions of complete and defective secondary structures, it is no surprise that the deactivation behavior is barely predictable. It is caused by short excursions of the control variables temperature and local gas composition that trigger the structural re-arrangements. The macroscopic picture is further complicated by a certain “repair” function of excessive water vapor acting as local hydrothermal synthetic agent on decomposed parts of the active material. Its function there is to provide locally sufficient partial pressure to complete the secondary structure and to hydrolyze the Mo-oligomers to allow the Keggin structure to re-form.

The role of vanadium as most beneficial addition to the Keggin structure has been found to allow the defect formation within the Keggin anion as “hemilabile” wall constituent and to help stabilizing defective Keggin units by forming vanadyl bridges in the secondary structure.

These functional views may not be transferred easily to other families of HPA compounds in particular those with tungsten in the Keggin unit. Other HPA may exhibit quite different patterns of metastability and hence different decomposition pathways. They then will act differently in catalysis and this may require different stability criteria. The present report has shown, however, that such information can be obtained on a significant level of precision by applying a set of in situ structural methods.

The ultimate use of the present family of HPA in catalysis is limited despite their great chemical variability, by their metastable nature that can only be overcome by stabilizing its secondary structure that hinders the formation of active sites. The dynamic nature of the defective active phase limits the predictability of the behavior of intermediate completion of the secondary structure that tends to disintegrate in core-and-shell states of complete and empty secondary structures.

References

1 M. Misono, N. Nojiri, Appl. Catal., 64 (1990) 1.
2 I.V. Kozhevnikov, Catal.Rev.Sci.Eng.,37, (1995), 311.
3 Th. Ilkenhans, B. Herzog, Th. Braun and R. Schlögl, J. Catal., 153 (1995) 275.
4 L. Weismantel, J. Stöckel and G. Emig, Appl. Catal., 137 (1996) 129.
5 K.-Y. Lee and M. Misono, in Handbook of Heterogeneous Catalysts, Ed. G. Ertl, H. Knözinger and J. Weitkamp,VCH, Weinheim, 1997, v.5, p.118.
6 T. Okuhara, N. Mizuno, and M. Misono, Adv. Catal. 41 (1996) 113.
7 M.T. Pope, Heteropoly and Polyoxometalates (Springer, Berlin, 1983).
8 M.Fournier, C. Lolouis, M. Che, P. Chaquin, D. Masure, J.Catal.,119, (1989), 400.
9 E. Cadot, C. Marchal, M. Fournier, A. Tezé, G. Hervé, Role of Vanadium in Oxidation Catalysis by Heteropolyanions, in: M.T. Pope, A.M. Müller (Eds), Polyoxometallates, Kluwer Academic Publishers, Dordrecht, 1994, pp.315 326.
10 J.K. Lee, J. Melsheimer, S. Berndt, G. Mestl, R. Schlögl, K. Köhler, Appl, Catal. A :General 214, (2001), 125.
11 J. Melsheimer, J. Kröhnert, R. Ahmad, S. Klokishner, F.C. Jentoft, G. Mestl, R. Schlögl, Phys.Chem.Chem.Phys., 4, (2002), 2398.
12 M. Thiede and J. Melsheimer, Rev. Sci. Instrum., 73, (2002), 1.
13 J.J. Altenau, M.T. Pope, R.A. Prados, and H. So, Inorganic Chemistry, (1975) 417.
14 G. Centi, J. Lopez Nieto and C. Iapalucci, Appl. Catal. 46, (1989), 197.
15 G. Centi, V. Lena, F. Trifiro, D. Ghoussoub, C.F. Aissi, M. Guelton and J.P. Bonnelle, J. Chem. Soc. Faraday Trans. 86, (1990), 2775.
16 D. Casarini, G. Centi, P. Jiru, V. Lena and Z. Tvaruzkova, J. Catal. 143, (1993) 325.
17 N.N. Timofeeva, A.V. Demidov, A.A. Davydov, I.V. Kozhevnikov, J. Mol. Catal., 79, (1993) 21.
18 J. Melsheimer, Sabri S. Mahmoud, G. Mestl and R. Schlögl, Catal. Lett., 60, (1999) 103.
19 S. Klokishner, J. Melsheimer, R. Ahmad, F. C. Jentoft, G. Mestl and R. Schlögl, Spectrochim. Acta, Part A, 58, (2002), 1.
20 T. Okuhara, N. Mizuno, M. Misono, Advances in Catalysis , 41, (2001), 443.
21 G. M. Brown, M.-R. Noe-Spirlet, W. R. Busing, H. A. Levy, Acta Cryst. ,B33, (1977),1038.
22 **a** N. Mizuno, D.-J. Suh, W. Han, T. Kudo, Journal of Mol. Catal. A 114, (1996), 309.
b N. Mizuno, M. Tateishi, M. Iwamoto, Appl. Catal. A, 118, (1994), L1.
c N. Mizuno, M. Tateishi, M. Iwamoto, Appl. Catal. A., 128, (1995), L165.
23 I. N. Staroverova, M. Yu. Kutyrev, L. G. Khvtisiashvili L.G., Kinetics and Katalysis 27, (1985), 596.
24 S. Berndt, D. Herein, F. Zemlin, E. Beckmann, G. Weinberg, J. Schütze, G. Mestl, R. Schlögl, Ber. Bunsenges. Phys. Chem. 102, (1998), 763.
25 J. B. Black, J. D. Scott, E. M. Serwicka, J B. Goodenough, J. Catal., 167, (1987), 16.
26 M. Langpape, J. M. M. Millet, U. S. Ozkan, M. Boudeulle, J. Catal., 181, (1999), 80.
27 J. B. Black, N. J. Clayden, P. L. Gai, J. D. Scott, E. M. Serwicka, J. B. Goodenough, J. Catal. ,106, (1987), 1.
28 F. Cavani, R. Mezzogori, A. Pigamo, F. Trifiro, E. Etienne, Catal. Today ,71, (2001), 97.
29 G. Mestl, T. Ilkenhans, D. Spielbauer, M. Dieterle, O. Timpe, J. Kröhnert, F. Jentoft, H. Knözinger, R. Schlögl, Appl. Catal. A, 210, (2001), 13.
30 C. Marchal-Roch, N. Laronze, N. Guilou, A. Teze, G. Herve, Appl. Catal. A , 199, (2000), 33.
31 C. Marchal-Roch, R. Bayer, J. F. Moisan, A. Teze, G. Herve, Topics in Catalysis, 3, (1996), 407.
32 G. Centi, V. Lena, F. Trifiro, D. Ghoussoub, C. F. Aissi, M. Guelton, J. P. Bonnelle, J. Chem. Soc. Faraday Trans.86, (1990), 2775.
33 O. Watzenberger, G. Emig, d. T. Lynch, J. Catalysis, 124, (1990), 247.
34 K. E. Lee, J. Melsheimer, S. Berndt, G. Mestl, R. Schlögl, K. Köhler, Appl. Catal. A, 214, (2001), 125.
35 L. Marosi, G. Cox, A. Tenten, H. Hibst, J. Catal.,194, (2000), 140.
36 S. Albonetti, F. Cavani, F. Trifiro, M. Gazzano, M. Koutyrev, F. C. Aissi, A. Aboukais, M. Guelton, J. Catal., 146, (1994), 491.
37 C. Marchal-Roch, J.-M. M. Millet, C.R. Acad. Sci., C4, (2001), 321.
38 M. Misono, Catal. Rev. – Sci. Eng. 29 (1987) 269.
39 T. Okuhara, T. Nishimura, H. Watanabe, and M. Misono, J. Mol. Catal. 74 (1992) 247.
40 LC. Jozefowicz, H.G. Karge, E. Vasilyeva, and J.B. Moffat, Microporous and Mesoporous Materials 1 (1993) 313.
41 N. Essayem, R. Frety, G. Coudurier, J.C. Vedrine, J. Chem. Soc. Faraday Trans. 93 (1997) 3243.
42 A. Bielański, A. Małecka, and L. Kubelkova, J. Chem. Soc. Faraday Trans. I 85 (1989) 2847.
43 F. Lefebvre, F.X.L. Cai, and A. Auroux, J. Mater. Chem. 4 (1994) 125.
44 G.I. Kapustin, T.R. Brueva, A.L. Klyachko, M.N. Timofeeva, S.M. Kulikov, and I.V. Kozhevnikov, Kinet. Katal. 31 (1990) 896.
45 M. Misono, N. Mizuno, K. Katamura, A. Kasai, Y. Konishi, K. Sakata, T. Okuhara, and Y. Yoneda, Bull. Chem. Soc. Jpn. 55 (1982) 400.
46 E.M. Serwicka, K. Bruckman, J. Haber, E.A. Paukshtis, and E.N. Yurchenko, Appl. Catal. 73 (1991) 153.
47 T. Okuhara, S. Tatematsu, K.Y. Lee, and M. Misono, Bull Chem. Soc. Jpn. 62 (1989) 717.
48 T. Saito, G. Koyano, and M. Misono, Chem. Lett. 11 (1998) 1075.
49 G. A. Tsigdinos, Topics in Current Chemistry, 76, (1987), 1.
50 T. Ressler, R. E. Jentoft, J. Wienold, M. M. Günter, O. Timpe, J. Phys. Chem B 104, (2000), 6360.
51 T. Ressler, J. Synch. Rad., 5, (1998), 118 .
52 J. J. Rehr, C. H. Booth, F. Bridges, S. I. Zabinsky, Phys. Rev., B 49, (1994), 12347.
53 D. Bassi, P. Tosi, R. Schlögl, J. Vac. Sci. Technol. A, 16, (1998), 114
54 L. Marosi, E. E. Platero, J. Cifre, C. O. Arean, J. Materials Chemistry, 10, (2000), 1949.
55 A. Jouanneaux, WinMProf: a visual Rietveld software, CPD newsletter, 21, (1999), 13.
56 T. Ressler, R. E. Jentoft, J. Wienold, T. Neisius, J. Catal., 210, (2002), 67.
57 M. T. Pope in Inorganic Chemistry Concepts, Vol. 8, (Hrsg.: C. K. Jørgensen, M. F. Lappert, S. J. Lippard, J. L. Margrave, K. Niedenzu, H. Nöth, R. W. Parry, H. Yamatera) Springer-Verlag, Berlin Heidelberg New York Tokyo, (1983), 59.

58 B.B. Bardin, S.V. Bordawekar, N. Neurock and R.J. Davis, J. Phys. Chem., 102, (1998), 10817.
59 H. Taneta, S. Katsuki, K. Eguchi, T. Seiyama and N. Yamazol, J. Phys. Chem., 90, (1986), 2959.
60 W. Feller, An introduction to probability theory and its applications, N.-Y., Wiley,1971.
61 H. Knözinger, Proc. of the Int. Symp. Acid-Base Catal. Sapporo 1988, Eds. K. Tanabe, H. Hattori, T. Yamaguchi, T. Tanaka,.
62 C. Rocchiccioli-Deltcheff, M. Fournier, R. Franck, and R. Thouvenot, Inorg. Chem. 22 (1983) 207.
63 C.D. Ai, P. Reich, E. Schreier, H.-G. Jerschkewitz, and G. Öhlmann, Z. anorg. allg. Chem. 526 (1985) 86.
64 C. Rocchiccioli-Deltcheff and M. Fournier, J. Chem. Soc. Faraday Trans. 87 (1991) 3913.
65 B.W.L. Southward, J.S. Vaughan, C.T. O'Connor, J. Catal. 153 (1995) 293.
66 C. Rocchiccioli-Deltcheff, A. Aouissi, M.M. Bettahar, S. Launay, and M. Fournier, J. Catal. 164 (1996) 16.
67 V. Sasca, M. Ştefănescu, A. Popa, J. Therm. Anal. Cal. 56 (1999) 569.
68 C. Knapp, T. Ui, K. Nagai, N. Mizuno, Catal. Today 71 (2001) 111.
69 N. Essayem, A. Holmqvist, P.Y. Gayraud, J.C. Vedrine, Y. Ben Taarit, J. Catal. 197 (2001) 273.
70 M.I. Zaki, B. Vielhaber, H. Knözinger, J. Phys. Chem. 90 (1986) 3176.
71 K. Eguchi, Y. Toyozawa, N. Yamazoe, T. Seiyama, J. Catal. 83 (1983) 32.